

# A Candidate multi-epitope vaccine against SARS-CoV-2

**Tamalika Ka**

Department of Life Sciences Garden City University Bangalore, Karnataka, India

**Utkarsh Narsaria**

Department of Life Sciences Garden City University Bangalore, Karnataka, India

**Srijita Basak**

Department of Life Sciences Garden City University Bangalore, Karnataka, India

**Debashrito De**

Department of Life Sciences Garden City University Bangalore, Karnataka, India

**Filippo Castiglioni**

Institute for Applied Computing National Research Council of Italy Via dei Taurini, Rome, Italy

**David M. Mueller**

Center for Genetic Diseases The Chicago Medical School Rosalind Franklin University of Medicine and Science  
North Chicago, USA

**Anurag P. Srivastava (✉ [anuiitkgp@gmail.com](mailto:anuiitkgp@gmail.com))**

Department of Life Sciences Garden City University Bangalore, Karnataka, India



---

**Research Article**

**Keywords:** SARS-CoV-2, spike glycoprotein, computational design, multi-epitope vaccine, Molecular Dynamics Simulation

**Posted Date:** May 9th, 2020

**DOI:** <https://doi.org/10.21203/rs.3.rs-28130/v1>

**License:**   This work is licensed under a Creative Commons Attribution 4.0 International License. [Read Full License](#)

---

**Version of Record:** A version of this preprint was published on July 2nd, 2020. See the published version at <https://doi.org/10.1038/s41598-020-67749-1>.

# Abstract

In the past two decades, 7 coronaviruses have infected the human population, with two major outbreaks caused by SARS-CoV and MERS-CoV in the year 2002 and 2012, respectively. Currently, the entire world is facing a pandemic of another coronavirus, SARS-CoV-2, with a high fatality rate. The spike glycoprotein of SARS-CoV-2 mediates entry of virus into the host cell and is one of the most important antigenic determinants, making it a potential candidate for a vaccine. In this study, we have computationally designed a multi-epitope vaccine using spike glycoprotein of SARS-CoV-2. The overall quality of the candidate vaccine was validated *in silico* and Molecular Dynamics Simulation confirmed the stability of the designed vaccine. Docking studies revealed stable interactions of the vaccine with Toll Like Receptors and MHC Receptors. Codon optimization was used to optimize high expression of the vaccine in *E.coli* K-12 strain. *In silico* cloning suggested efficient expression in pET-28a (+) vector. The efficiency of the candidate vaccine to trigger an effective immune response was assessed by an *in silico* immune simulation. The computational analyses suggest that the designed multi-epitope vaccine is structurally stable which can induce specific immune responses and thus, can be a potential vaccine candidate against SARS-CoV-2.

Authors Tamalika Kar, Utkarsh Narsaria, Srijita Basak, and Debashrito Deb contributed equally to this work.

## Introduction

Wuhan, a city in China, witnessed the outbreak of a febrile respiratory illness on 19th December 2019 due to the coronavirus provisionally named as 2019-nCoV and later SARS-CoV-2 [1, 2]. The disease caused by coronavirus was named as COVID-19 [1, 2]. Since then, the world is experiencing a grave situation of global public health emergency due to the viral pandemic of severe febrile pneumonia like respiratory syndrome caused by the novel coronavirus [2]. Coronaviruses are known to have caused three epidemics in the last two decades, namely COVID-19 in 2019/20, Severe Acute Respiratory Syndrome (SARS) in 2002, and Middle East Respiratory Syndrome (MERS) in 2012 [3]. As of April 15<sup>th</sup> 2020, total cases of SARS-CoV-2 confirmed globally by World Health Organization are 1,914,916 with 123,010 reported deaths (<https://www.who.int/emergencies/diseases/novel-coronavirus-2019/situation-reports>).

Human coronavirus (H-CoV) is a member of Coronaviridae family, a virus family characterized with the largest RNA genome (26–32kb), among all of the viruses known till date [4–6]. A lipid envelope bilayer containing the spike and membrane proteins surround positive stranded RNA genome of this virus [7]. The spike protein binds to the host cell receptors and releases the viral genome into the host cell, thereby facilitating the viral replication [8]. Corona Viruses (CoVs) are mostly associated with respiratory illness and common cold [9], but can also cause infections in Central Nervous System (CNS) [10]. To date, four genera of coronaviruses ( $\alpha$ ,  $\beta$ ,  $\gamma$ ,  $\delta$ ) have been identified [11]. Human coronaviruses (H-CoVs) belongs to  $\alpha$  (HCoV-229E and NL63) and  $\beta$  (MERS-CoV, SARS-CoV, HCoV-OC43, HCoV-HKU1 and SARS-CoV-2) genera of coronavirus, respectively [11].

In late December 2019, patients with Acute Respiratory Distress Syndrome (ARDS) along with cough, fever and dyspnoea due to an unknown microbial infection were recorded in Wuhan, China [12]. Viral genome sequencing of five pneumonia patients, hospitalized between 18<sup>th</sup> December and 29<sup>th</sup> December 2019, reported the presence of a previously unknown  $\beta$ -CoV strain in all of the 5 hospitalized patients [12]. There was around 88% sequence similarity between the novel  $\beta$ -CoV strain and two bat-derived severe acute respiratory syndromes (SARS)-like

coronaviruses namely, bat-SL-CoVZC45 and bat-SL-CoVZXC21, while MERS-CoV displayed a sequence identity of about 50% with the novel  $\beta$ -CoV [12].

Coronavirus infection in humans is primarily guided by interactions between envelope anchored spike glycoprotein (S-protein) of CoV and angiotensin converting enzyme 2 (ACE2) of the host cell receptor [13, 14]. The viral RNA genome is released into the cytoplasm after the virus enters the cells and is then translated into two polyproteins and structural proteins, after which the viral genome starts to replicate [11]. The S protein is composed of two subunits, one subunit, S1, is the Receptor Binding Domain (RBD) and the other subunit, S2, is responsible for the fusion of viral membrane and the host cellular membrane [15]. An overall 75% sequence similarity was seen between SARS-CoV-2 and previously identified SARS-CoV spike protein [16, 17] and it is also reported, that the Coronavirus S protein is a major determinant of virus entry into host cells [3]. Hence, the spike like glycoprotein is a potent choice for vaccine designing.

The conventional method of vaccine designing, involving the entire organisms or large proteins leads to unnecessary antigenic load along with increased chances of allergenic responses [18]. This problem can be overcome by peptide based vaccines comprising short immunogenic peptide fragments with the ability to elicit strong and targeted immune responses, avoiding the chances of allergenic reactions [18]. Recent advancements in computational biology have opened up new doors for designing effective vaccines *in silico*. [19–21]. In this study, the *in silico* approach has been applied for attaining a multi-epitope vaccine against SARS-CoV-2 that comprises epitopes of spike glycoprotein epitopes which induces the activation of cytotoxic T lymphocytes (CTLs), helper T lymphocytes (HTLs) and interferon- $\gamma$  (IFN- $\gamma$ ) (Fig. 1).

## Results

### Sequence retrieval and Phylogenetic analysis

The spike glycoprotein sequence of SARS-CoV-2 was retrieved from PDB (6VSB). Phylogenetic analysis showed that the glycoprotein variants of SARS-CoV-2 clustered together in a single clade, having the most common ancestry with SARS-CoV and MERS-CoV (Fig. 2). The variants of SARS-CoV-2 that clustered together had very less branching, indicating low mutation rate. Hence, the vaccine designed against one strain can be used for all the other strains of SARS-CoV-2. The phylogenetic analysis of all the glycoproteins of different strains of SARS-CoV-2, isolated from different countries indicated that all the glycoproteins were closely related to one another (Supplementary Fig. 1).

### T cell epitope prediction

CTL epitopes were predicted using NetCTL1.2 and IEDB consensus methods whereas, HTL epitopes were predicted using NetMHC II pan 3.2 server as shown in Table 1 and Table 2 (Supplementary Table 1 and 2). To identify the best epitopes, the predicted epitopes were subjected to various immune filters and those having high binding affinity to MHC class I and class II alleles were selected. The criteria for screening out the epitopes were: they should be promiscuous, should be antigenic and should be immunogenic. The antigenicity of the epitopes was predicted using VaxiJen v2.0 and immunogenicity was predicted using IEDB class I immunogenicity server. The 3D structure of spike glycoprotein was modelled using I-TASSER and the epitopes considered for vaccine construction were visualized on the same (Fig. 3).

**Table 1:** CTL epitopes predicted using NetCTL 1.2 showing promiscuity. Epitopes with IC50 value <500nm were considered good binders towards specific alleles. VaxiJen v2.0 was used for predicting antigenicity scores keeping a threshold of 0.4.

EPITOPES	SUPERTYPE	MHC CLASS I ALLELE	BINDING SCORE	IC50	POSITION	PREDICTION SCORE	IMMUNOGENIC SCORE	ANTIGENIC SCORE
QIITDNTF	A24,A26,B58, B62	HLA-B*15:01	1.3	66.32	1113	0.7939	0.15816	0.4253
		HLA-A*32:01	1.7	472.54				
YQPYRVVVL	A2,A24,B8,B3 9,B62	HLA-B*15:01	1.2	131.99	505	0.8143	0.1409	0.5964
		HLA-A*02:06	1.615	99.74				
FTISVTTEI	A2,A26,B58	HLA-A*68:02	0.2	3.05	718	1.1808	0.04473	0.8535
		HLA-B*58:01	0.4	48.78				
		HLA-A*02:06	0.6	8.29				
		HLA-A*26:01	0.615	481.17				
		HLA-A*02:01	0.8	25.37				
		HLA-A*02:03	0.94	9.07				
YLQPRTFLL	A2,B8,B39	HLA-A*02:01	0.3	5.36	269	1.5152	0.1305	0.4532
		HLA-A*02:06	0.96	16.55				
		HLA-B*08:01	1.0	147.76				
		HLA-A*02:03	1.005	15.24				
		HLA-A*24:02	1.115	406.74				
		HLA-A*23:01	1.275	278.62				
HSAWHPQF	A1A24,B39,B5 8,B62	HLA-B*58:01	0.5	17.5	1257	0.8279	0.0279	0.8569
		HLA-B*35:01	1.5	287.84				
STQDLFLPF	A1,A26,A24,B 62	HLA-A*32:01	0.2	17.27	50	1.0468	0.06828	0.6619
		HLA-B*15:01	0.3	13.32				
		HLA-A*26:01	0.46	437.88				
		HLA-A*23:01	1.415	394.77				
WTAGAAAYY	A1,A26,B58,B 62	HLA-A*26:01	0.11	11.63	258	3.1128	0.15259	0.6306
		HLA-A*30:02	0.115	16.16				
		HLA-A*01:01	0.17	12.27				
		HLA-A*68:01	1.185	30.13				
		HLA-B*35:01	1.2	66.67				
		HLA-B*15:01	1.6	132.2				

**Table 2:** HTL epitopes showing promiscuity, as predicted using NetMHC II pan 3.2 server. VaxiJen v2.0 was used for predicting antigenicity scores keeping a threshold of 0.4

EPITOPES	POSTION	ALLELE	SCORE	ANTIGENIC SCORE
INITRFQTLALHRS	233	DRB1*01:01	1.00	0.418
		DRB1*04:01	0.80	
		DRB1*04:05	0.25	
		DRB1*08:02	1.60	
		DRB1*11:01	0.60	
		DRB1*12:01	0.90	
		DRB1*15:01	0.30	
		DRB4*01:01	0.50	
		DPA1*02:01-DPB1*05:01	0.40	
		DPA1*02:01-DPB1*14:01	0.70	
		DRB5*01:01	0.12	
GINITRFQTLALHR	232	DRB1*01:01	1.60	0.5582
		DRB4*01:01	0.50	
		DRB5*01:01	0.30	
		DPA1*03:01-DPB1*04:02	2.00	
		DPA1*02:01-DPB1*05:01	0.50	
		DPA1*02:01-DPB1*14:01	1.00	
		DPA1*02:01-DPB1*01:01	1.60	
		DRB1*04:01	1.00	
		DRB1*04:05	0.25	
		DRB1*11:01	1.30	
		DRB1*12:01	0.80	
GWTFGAGAALQIPFA	885	DRB1*15:01	0.25	0.4665
		DRB1*01:01	2.00	
		DRB1*09:01	0.20	
		DQA1*03:01-DQB1*03:02	0.60	
		DQA1*04:01-DQB1*04:02	0.40	
IRAAEIRASANLAAT	1013	DQA1*01:02-DQB1*06:02	0.60	0.6785
		DQA1*05:01-DQB1*03:01	0.10	
		DRB1*04:01	1.40	
		DRB1*08:02	1.20	
		DRB1*13:02	1.90	
AAEIRASANLAATKM	1015	DPA1*02:01-DPB1*14:01	0.80	0.7125
		DQA1*01:02-DQB1*06:02	0.30	
		DQA1*05:01-DQB1*03:01	1.00	
		DRB1*04:01	0.70	
		DRB1*08:02	0.70	
WTFGAGAALQIPFAM	886	DRB1*13:01	1.10	0.6670
		DPA1*02:01-DPB1*14:01	0.50	
		DQA1*01:02-DQB1*06:02	1.30	
		DRB3*02:02	1.10	
		DRB1*09:01	0.40	
QPYRVVLSFELLHA	506	DQA1*03:01-DQB1*03:02	0.80	0.9109
		DQA1*04:01-DQB1*04:02	0.50	
		DQA1*01:02-DQB1*06:02	0.50	
		DQA1*05:01-DQB1*03:01	0.17	
		DPA1*02:01-DPB1*01:01	0.70	
PYRVVLSFELLHAP	507	DPA1*01:03-DPB1*04:01	1.10	0.8161
		DPA1*03:01-DPB1*04:02	0.50	
		DPA1*02:01-DPB1*05:01	0.80	
		DPA1*01:03-DPB1*02:01	1.10	
		DPA1*02:01-DPB1*01:01	0.80	
PYRVVLSFELLHAP	507	DPA1*01:03-DPB1*02:01	1.30	0.8161
		DPA1*03:01-DPB1*04:02	0.60	
		DPA1*02:01-DPB1*05:01	0.80	
		DPA1*01:03-DPB1*04:01	1.30	

## Multi epitope vaccine construct, Structural Modeling, Refinement and Validation

The main criteria used for designing the linear vaccine construct were: 1. it should contain overlapping HTL and CTL epitopes (Supplementary Table 3), 2. It must be immunogenic, antigenic, but not an allergen, 3. It should have high affinity to HLA alleles and should be promiscuous. On basis of these parameters, a linear vaccine was constructed including 7 CTL, 8 HTL and 3 IFN- $\gamma$  (Table 1, Table 2 and Supplementary Table 4) epitopes joined by GPGPG linkers. Cholera Toxin B (CTB) adjuvant was attached to the N-terminal of the construct via EAAK linker (Fig. 4A). The final vaccine construct consisted of 422 amino acids with a molecular weight of 44.15 kDa. The 3D

models of the vaccine were generated using trRosetta server (Fig. 4B). Amongst the predicted models, the best model was chosen that had a Z-score of -8.1 and it was within the range of scores of comparable size proteins [22] (Fig. 4D). Ramachandran plot analysis showed 96.4%, 2.9% and 0.7% residues in favoured, allowed and outlier regions, respectively which further verified the overall quality of the vaccine construct (Fig. 4E). The ERRAT of the refined structure revealed an overall score of 74.2947 (Fig. 4C).

## Physicochemical properties of the vaccine construct

The multi-epitope vaccine construct was found to be immunogenic as predicted by IEDB class I immunogenicity tool with a score of 6.65414. VaxiJen v2.0 confirmed the antigenicity of the vaccine with a score of 0.5107. Allergenicity was checked and it was found to be non- allergen as predicted by AllerTOP and AllergenFP web servers. Other physicochemical properties were evaluated using ExPASy (Supplementary Material 1), which revealed the theoretical pI and aliphatic index of the vaccine to be 9.96 and 78.74, respectively. The estimated half-life of the vaccine as predicted by ExPASy is 30 hours in mammalian reticulocytes, >20 hours in yeast and >10 hours in *Escherichia coli*. The Grand average hydropathicity (GRAVY) is -0.088, which supports the polar nature of the candidate vaccine. The instability index of candidate was found to be 31.04, indicating the protein to be a stable one. Since the designed candidate construct does not contain any transmembrane helices, no expression difficulties are anticipated in the production of vaccine (Supplementary Figure S3). Also, the absence of signal peptides in the vaccine construct signifies prevention of protein localization (Supplementary Figure S2).

## B cell epitope prediction

The linear/continuous and conformational/discontinuous B cell epitopes were predicted by the ElliPro server using default parameters (Table 3 and Table 4). The visualisation of B cell epitopes in the final vaccine construct was done using PyMOL (The PyMOL Molecular Graphics System, Version 2.0 Schrödinger, LLC.) (Supplementary Figure S4).

**Table 3:** Conformational/ Discontinuous B cell epitopes in the multi-epitope vaccine, predicted by ElliPro server.

DISCONTINUOUS EPITOPES	SCORE
R(334), KMGPGGTRFAS(361-372), YAWNRRK(374-379), ISGPGGGINITRFQTLAL(381-400), RGPGGINI(402-410), RFQTLAL(412-419), RS(421-422)	0.766
M(1), DLCAEYHNTQIH(8-19), FSYTESLAGKREMAII(26-41), F(43), NGATFQVEVPGSQHIDSQKKAIERMKDTRLIA(45-76), LT(78-79), AKVEKLCV(81-88), NNK(90-92), PHAIAA(94-99), SM(101-102)	0.752
HAGPGPGPY(261-269), AGPGPGW(302-308)	0.647
L(114), YGPGPYL(131-139), GPGPGF(161-166), DNTFGPGPGHS(185-195), S(198)	0.608
FAMGPGGIRA(320-330)	0.601
LPFGPGGWT(116-125), W(197), FGPGPG(202-207)	0.579
ATGPGGAAE(341-350)	0.522

**Table 4:** Linear/ continuous B cell epitopes in the Vaccine construct, predicted by ElliPro server.

LINEAR EPITOPES	POSITION	SCORE
FSYTESLAGKREMAII	26	0.824
AWNRRKRISGPGPGGINITRFQTLALHRGPGPGINITRFQTLALHRS	375	0.81
GATFQVEVPGSQHIDSQKKAIERMKDTRLRIAYLTEAKVEKLCVWNNKTPHAIAAIS M	46	0.745
HAGPGPGPY	261	0.731
KMGPGPGTRFA	361	0.721
DLCAEYHNTQIH	8	0.718
FGPGPGWT	118	0.666
YGGPGPGYL	131	0.655
FAMGPGPGIR	320	0.618
TFGPGPGHSAWSHPQFGPGP	187	0.602
AGPGPG	302	0.561
ATGPGPGAA	341	0.546
GPGPG	161	0.543
HRGPGPG	221	0.526

## Population Coverage

The selected epitopes showed a total world population coverage of 95.78% (Table 5). In addition, the epitopes showed 97.47%, 97.26%, 84.84%, 87.66% and 90.77% coverage in Europe, United States, China, South Asia and Oceania, respectively (Table 5) (Supplementary Figure S5). The results suggest that the designed multi-epitope vaccine can be used to tackle SARS-CoV-2 globally.

**Table 5:** Population coverage of the selected epitopes of the vaccine construct, as predicted by IEDB server.

Population/area	Coverage	Average hit	pc90
World	95.78	4.29	1.78
Europe	97.47	4.69	2.14
United States	97.26	4.69	2.14
China	84.84	3.17	0.66
South Asia	87.66	3.1	0.81
Oceania	90.77	2.79	1.04

## Molecular Docking Analysis- Docking of the vaccine with TLR4

HADDOCK clustered 33 structures in 7 cluster(s), which represents 16.5% of the water refined HADDOCK generated models. The top cluster with the lowest HADDOCK score is the most reliable cluster of all. A representative model of the top cluster was subjected to further refinement using HADDOCK refinement server, where 20 structures were clustered into one cluster, resulting in 100% of the water refined models generated by HADDOCK. The statistics of the refined model are presented in the Table 6, and the structural analysis of the refined model is shown in Supplementary Figure S7. The predicted interaction of the amino acids and a detailed overview of the molecular docking are given in Supplementary Material 2 and Supplementary Figure S8, respectively. Also, Ramachandran plot analysis was carried out for structural validation of the docked complex (Supplementary Figure S6). The docked complex along with the some prominent hydrogen bonds is shown in Figure 5.

**Table 6:** Table showing statistics of best refined docked TLR4/MD2 and vaccine complex. Smaller HADDOCK score represents strong protein interaction which is expressed in arbitrary units (a.u).

Vaccine-TLR4	
HADDOCK score (a.u)	-130.9 +/- 10.1
Cluster size	20
RMSD from the overall lowest-energy structure (Å)	0.3 +/- 0.2
Van der Waals energy (kcal mol <sup>-1</sup> )	-72.4 +/- 1.3
Electrostatic energy ( kcal mol <sup>-1</sup> )	-238.9 +/- 12.2
Desolvation energy ( kcal mol <sup>-1</sup> )	-10.9 +/- 13.2
Restraints violation energy ( kcal mol <sup>-1</sup> )	1.1 +/- 0.44
Buried Surface Area (Å <sup>2</sup> )	2204.4 +/- 22.4

## Docking of vaccine with TLR2

HADDOCK clustered 80 structures in 11 cluster (s), which represents 40.0% of the water refined HADDOCK generated models. The structure with the lowest HADDOCK score was chosen as the top cluster. A representative model of the top cluster was subjected to further refinement using HADDOCK refinement server, where 20 structures were clustered into one cluster, resulting in 100% of the water refined models generated by HADDOCK. The statistics of the refined model are presented in the Table 7, and the structural analysis of the refined model is shown in Supplementary Figure S10. The predicted interaction of the amino acids and a detailed overview of the molecular docking are given in Supplementary Material 3 and Supplementary Figure S11, respectively. Also, Ramachandran plot analysis was carried out for structural validation of the docked complex (Supplementary Figure S9). The docked complex along with the some prominent hydrogen bonds is shown in Figure 6.

**Table 7:** Table showing statistics of best refined docked TLR2 and vaccine complex. Smaller HADDOCK score represents strong protein interaction which is expressed in arbitrary units (a.u).

Vaccine-TLR2	
HADDOCK score (a.u)	-112.0 +/- 2.8
Cluster size	20
RMSD from the overall lowest-energy structure (Å)	0.3 +/- 0.2
Van der Waals energy (kcal mol <sup>-1</sup> )	-73.2 +/- 5.2
Electrostatic energy ( kcal mol <sup>-1</sup> )	-319.7 +/- 32.7
Desolvation energy ( kcal mol <sup>-1</sup> )	25.1 +/- 4.3
Restraints violation energy ( kcal mol <sup>-1</sup> )	0.0 +/- 0.00
Buried Surface Area (Å <sup>2</sup> )	2094.7 +/- 24.1

## Docking of vaccine with MHC class I receptor

HADDOCK clustered 120 structures in 12 cluster(s), which represents 60.0% of the water refined HADDOCK generated models. The structure with the lowest HADDOCK score was chosen as the top cluster. A representative



model of the top cluster was subjected to further refinement using HADDOCK refinement server, where 20 structures were clustered into one cluster, resulting in 100% of the water refined models generated by HADDOCK. The statistics of the refined model are presented in the Table 8, and the structural analysis of the refined model is shown in Supplementary Figure S13. The predicted interaction of the amino acids and a detailed overview of the molecular docking are given in Supplementary Material 4 and Supplementary Figure S14, respectively. Also, Ramachandran plot analysis was carried out for structural validation of the docked complex (Supplementary Figure S12). The docked complex along with the some prominent hydrogen bonds is shown in Figure 7.

**Table 8:** Table showing statistics of best refined docked MHC class I and vaccine complex. Smaller HADDOCK score represents strong protein interaction which is expressed in arbitrary units (a.u).

Vaccine-MHC I	
HADDOCK score (a.u)	-214.7 +/- 4.1
Cluster size	20
RMSD from the overall lowest-energy structure (Å)	0.3 +/- 0.2
Van der Waals energy (kcal mol <sup>-1</sup> )	-138.5 +/- 2.2
Electrostatic energy (kcal mol <sup>-1</sup> )	-156.3 +/- 16.9
Desolvation energy (kcal mol <sup>-1</sup> )	-45.0 +/- 5.8
Restraints violation energy (kcal mol <sup>-1</sup> )	0.0 +/- 0.00
Buried Surface Area (Å <sup>2</sup> )	3585.9 +/- 60.3

## Docking of vaccine with MHC class II receptor

HADDOCK clustered 64 structures in 9 cluster (s), which represents 32% of the water refined HADDOCK generated models. The structure with the lowest HADDOCK score was chosen as the top cluster. A representative model of the top cluster was subjected to further refinement using HADDOCK refinement server, where 20 structures were clustered into one cluster, resulting 100% of the water refined HADDOCK generated models. The statistics of the refined model are presented in the Table 9, and the structural analysis of the refined model is shown in Supplementary Figure S16. The predicted interaction of the amino acids and a detailed overview of the molecular docking are given in Supplementary Material 5 and Supplementary Figure S17, respectively. Also, Ramachandran plot analysis was carried out for structural validation of the docked complex (Supplementary Figure S15). The docked complex along with the some prominent hydrogen bonds is shown in Figure 8.

**Table 9:** Table showing statistics of best refined docked MHC class II and vaccine complex. Smaller HADDOCK score represents strong protein interaction which is expressed in arbitrary units (a.u).

Vaccine-MHC II	
HADDOCK score (a.u)	-212.1 +/- 2.2
Cluster size	20
RMSD from the overall lowest-energy structure (Å)	0.3 +/- 0.2
Van der Waals energy (kcal mol <sup>-1</sup> )	-132.5 +/- 3.2
Electrostatic energy (kcal mol <sup>-1</sup> )	-394.9 +/- 42.3
Desolvation energy (kcal mol <sup>-1</sup> )	-0.6 +/- 4.4
Restraints violation energy (kcal mol <sup>-1</sup> )	0.2 +/- 0.27
Buried Surface Area (Å <sup>2</sup> )	4276.9 +/- 43.1

## Binding Affinity Analysis

The binding affinity of the 4 docked complexes was analysed using PRODIGY web server. The results revealed that all of the 4 dockings were energetically feasible, as indicated by the negative values of Gibbs free energy ( $\Delta G$ ). The  $\Delta G$  values for the vaccine-TLR4, vaccine-TLR2, vaccine-MHC class I and vaccine-MHC class II receptor was found to be  $-10.3 \text{ kcal mol}^{-1}$ ,  $-11.2 \text{ kcal mol}^{-1}$ ,  $-13.5 \text{ kcal mol}^{-1}$ ,  $-16.0 \text{ kcal mol}^{-1}$ , respectively (Table 10). The dissociation constant ( $K_d$ ) of the docked complexes are shown in Table 10.

**Table 10:** Binding affinities of the docked complexes of the vaccine with TLR4, TLR2, MHC I and MHC II, as predicted by PRODIGY server.

Complexes	Gibbs Free Energy (kcal mol <sup>-1</sup> )	Kd (M)
Vaccine-TLR4	-10.3	5.3E-08
Vaccine-TLR2	-11.2	1.3E-08
Vaccine-MHC class I receptor	-13.5	2.9E-10
Vaccine-MHC class II receptor	-16	5.0E-12

## Energy minimization and Molecular Dynamics Simulation of the vaccine construct

Energy minimization for the vaccine construct was conducted for 2262 steps where the force reached  $<1000 \text{ kJ/mol}$ . The potential energy of the system was computed to be  $-3.0 \times 10^6 \text{ kJ/mol}$  with a total drift of  $-3.8 \times 10^5 \text{ kJ/mol}$  and the average potential energy was  $-2.9 \times 10^6 \text{ kJ/mol}$ . After 50,000 steps of NVT the average temperature was 299.8K with a drift of 1.0K (Fig. 9D). The average density of the system computed was  $1012.5 \text{ kg/m}^3$  with a total drift of  $1.3 \text{ kg/m}^3$  (Fig. 9B). The pressure of the system was found to be 1.6 bar with a total drift of

4.2 bar (Fig. 9C). Trajectory analysis was performed after a simulation period of 10 ns. The plot for the radius of gyration showed the compactness of the protein around its axes (Fig. 9A). A plot of RMSD backbone revealed very mild fluctuations, indicating the stability of the vaccine over time (Fig. 9E). The high peaks in the RMSF plot suggested a high degree of flexibility in the vaccine construct (Fig. 9F).

# Reverse translation, codon optimization and *in silico* cloning of the vaccine

The codon optimization index (CAI) is 1.0 and GC content of the reverse translated vaccine is 58.53%. These results support the proficient expression of the designed vaccine in *E. coli* strain K-12 host. The cDNA obtained after reverse translation of the designed multi-epitope vaccine was inserted into pET-28a (+) vector for restriction cloning (Figure 10).

## Immune simulation

The *in silico* immune response generated by the C-IMMSIM immune server is shown in Figure 11. The secondary and tertiary responses generated by the simulation were significantly higher when compared to the primary response. The secondary and tertiary responses revealed a decrease in the antigenic concentration with normal high levels of immunoglobulin activity (i.e., IgG1+IgG2, IgM, and IgG+IgM antibodies). In addition, multiple long lasting B cell isotypes were found, suggesting possible isotype switching potentials and memory formation (Fig. 11 panel A ii, Supplementary Figure S18). The TH (helper) and TC (cytotoxic) cell populations also showed a similar higher response with the pre activation of TCs during vaccination (Fig. 11 panel Aiv and panel Aiii) (Supplementary Figure S17 F and S17 B). The NK (natural killer) and dendritic cell activity was found to be consistent along with higher macrophage activity (Supplementary Figure S18) demonstrated during the exposure (Fig. 11 panel Av). The generation of a good immune response was supported by the high levels of IFN- $\gamma$  and IL-2 elicited in the simulation. After the vaccination, an injection of a “live-replicating virus” was simulated at around day 366 in order to check the efficacy of the vaccine. The antigen graph (Fig. 11 panel Ai) shows that after the vaccination, when a live replicating virus is injected, the antigenic surge is virtually absent, indicating an effective immune response mainly due to the protective action of high concentration of specific antibodies. This outcome should be compared with a control simulation that was also performed consisting of an injection of the live virus after 1 year, without prior vaccination. In this case, results indicate that without prior vaccination the host is unable to contain the antigen, though an inefficacious immune response is generated (Fig. 11B, Supplementary Figure S19).

## Discussion

SARS-CoV-2 has been declared as a global pandemic by the World Health Organization affecting people of all age groups. World Health Organization’s announcement on COVID-19 as a global public health emergency has encouraged researchers to develop therapeutics such as drug candidates and vaccines against the disease [23]. The cost effective and time saving immunoinformatic approaches have already helped the researchers to predict potential antigenic epitopes required for the development of a multi-epitope vaccine candidate [24-27]. The distinctive concept of multi-epitope vaccine design as compared to classical single-epitope based vaccine is that, the screening of viral genome to identify immunogenic epitopes results in the elicitation of a highly targeted immune response without any reversal of viral pathogenesis [28].

In this study, we aim at designing a multi-epitope, prophylactic vaccine targeting the spike protein of SARS-CoV-2, which is one of the major determinants of antigenicity and viral entry into the host cell [3]. Several computational tools were used to construct a multi-epitope vaccine, which has the ability to generate both humoral and cell mediated immunity. The multi-epitope vaccine elicits immune responses based on short immunogenic sequences instead of large proteins or whole genome which is typically used for recombinant vaccine technology. Thus, this approach avoids the excess antigenic load as well as allergenic responses in the host [18, 29, 30]. The analysis of the entire spectrum of possible antigens can be carried out using immunoinformatics and molecular modeling in order to examine the potential binding with host proteins [24, 31-34]. In addition, these multi-epitope vaccines have advantages over traditional and single-epitope vaccines due to the following unique features: i) multiple MHC Class I and Class II epitopes can be recognized by TCRs from various T cell subsets, ii) overlapping CTL, HTL and B cell epitopes have the capacity to activate humoral and cellular immune responses simultaneously, iii) linking an adjuvant to the vaccine ensures a long lasting immune response with enhanced immunogenicity, iv) the *in vitro* antigen expression complications as well as the difficulty of culturing the pathogens can also be avoided [35-43]. Designing of multi-epitope vaccines is an emerging area which has already gained importance, and the vaccines designed by this approach, have not only shown *in vivo* efficacy with protective immunity [44-46] but also entered phase-I clinical trials [39, 40, 47, 48].

The present study utilized the potential immunogenic epitopes identified from the SARS-CoV-2 spike protein to construct the multi-epitope vaccine with Cholera Toxin B (CTB) as an adjuvant along with appropriate linkers. Cholera Toxin B, which has been proven to act as a potential viral adjuvant, is linked at the N-terminal of the vaccine construct [49-51].

Glycine rich linker, such as GPGPG, was preferred to link the screened epitopes as it enhances the solubility and enable the adjoining domains to be accessible and act freely [52]. Various immunological filters were used to screen the predicted CTL and HTL epitopes: the epitopes must be antigenic and immunogenic, should bind with multiple MHC class I and MHC class II alleles (promiscuous), and must have overlapping CTL and HTL epitopes. Our designed vaccine was predicted to be non-allergen using AllerTOP v.2.0 server which was further verified by AllergenFP v.1.0 [53, 54]. The other physicochemical properties of the vaccine were analysed using ProtParam tool offered by Expasy server [55]. The molecular weight of the construct was 44.15kDa and the instability index was evaluated to be 31.04 which classify the vaccine to be stable. Generally, a protein whose instability index is lesser than 40 are predicted to be stable and values above that predicts the protein as unstable [55]. The stability of the vaccine candidate in this study was found to be better than the recently published multiepitope vaccine candidate against SARS-CoV-2 in which instability index was found higher than the vaccine candidate of this study [56, 57]. The theoretical pI of the vaccine was calculated to be 9.96. The GRAVY index of the vaccine was -0.088, (lower the GRAVY score, better is the solubility), which is reflective of the vaccine's polar nature and its effective interaction with water, suggesting high solubility [58]. The designed vaccine in this study has better solubility when compared to the other vaccine candidates proposed against SARS-CoV-2 by other research groups, Rehman et al., and Qamar et al., where the GRAVY score was found to be 0.158 and 0.105, respectively. The aliphatic index of 78.74 indicated the protein to be thermostable [59]. The half-life of the vaccine was evaluated to be 30 hours (mammalian reticulocytes, *in vitro*), >20 hours (yeast, *in vivo*) and >10 hours (*Escherichia coli*, *in vivo*) which indicates the time taken by the protein to reach 50% of its concentration after its synthesis in the cell. The structural validation of the vaccine construct performed by Ramachandran plot analysis using RAMPAGE showed that 96.4% of residues were in favoured region, 2.9% were in the allowed region and only 0.4% of the residues were placed in the outlier region thereby, validating the tertiary structure of the vaccine. The ERRAT score of 74.29

further validated the overall quality of the vaccine and Z-score assessment by ProSA web server revealed a score of -8.1, indicating that the protein falls in the plot which consists of the Z-scores of the already determined structures solved by NMR and X-ray crystallographic experiments [22].

The spike glycoprotein of SARS-CoV-2, which is one of the structural components of the virus, should be recognized by the Toll Like Receptor 4 (TLR4) and Toll Like Receptor 2 (TLR2) expressed in the plasma membrane of the cells [60-62]. Human Toll Like Receptor 4 (TLR4) is expressed in various types of immune cells like monocytes, macrophages, granulocytes and immature dendritic cells [63]. A direct interaction between TLR4 and CTB is responsible for the activation of TLR4 by CTB [64]. This conclusion is strengthened by the fact that the capacity of CTB to induce inflammatory response is lost in TLR4-deficient macrophages [64]. The ELISA-based assays have demonstrated that CTB is able to induce NF- $\kappa$ B activation in TLR4 receptor cells by binding to it directly [64]. In addition, TLR2 is also associated with recognition of viral envelop glycoprotein [60]. The myeloid differentiation factor 88 (MyD88) acts as the primary adaptor for the core TLR2 signalling pathway, which results in NF- $\kappa$ B and mitogen-activated protein kinase (MAPK) activation, leading to secretion of a core panel of cytokines [60]. The interaction pattern of the vaccine with TLR4 and TLR2 was analysed by Molecular Docking Studies (Fig. 5 and Fig. 6). The docking analysis of TLR4 and the vaccine construct showed that there are 3 salt bridges and 7 hydrogen bonds formed during this interaction. The docked complex shows that the salt bridges were formed between Arg41, Glu68, Asp69 of TLR4 and Asp113, Lys85, Lys82 of vaccine, respectively. Similarly, docking analysis of TLR2 and the vaccine construct also showed that there are 3 salt bridges and 9 hydrogen bonds formed during the interaction. The salt bridges formed in this case were between Asp516, Asp520, Arg547 of TLR4 and Lys85, Lys82, Glu105 of our vaccine, respectively. The molecular dynamics simulation of the vaccine construct for 10ns showed that there were very mild fluctuations in the RMSD graph, indicating the vaccine's stability (Fig. 9). The RMSF graph showed regions with high peaks, indicating the high flexibility of the vaccine construct (Fig. 9). To assure an effective expression, the linear vaccine construct was reverse translated into its specific cDNA sequence. The GC content of it was recorded as 58.53%, therefore showing the possibility of efficient expression of the vaccine in candidate *E. coli* host. Further, insertion of the vaccine in the expression vector pET-28a (+) for *in silico* cloning was performed for expression of the vaccine in bacterial system. The immune simulation studies confirmed that the designed vaccine was able to elicit specific immune responses required to clear the antigen on secondary exposure (Fig. 11). Similar strategy has recently been applied for designing multi-epitope vaccines against *Pseudomonas aeruginosa* [65], *Klebsiella pneumoniae* [66], Dengue [67], Nipah virus [68], Hendra virus [69] and Malaria [70]. In addition, similar approach has also been applied for developing vaccine against cancerous antigens [18, 71]. The CTL, HTL and IFN- $\gamma$  epitopes included in the vaccine has the capacity to trigger the stimulation of host's respective immune cells which in turn can cause the activation of other immune cells via complex signalling.

## Materials And Methods

### Sequence retrieval and phylogenetic tree construction

The VIPR database (<https://www.viprbrc.org/brc/home.spg?decorator=vipr>) was used to retrieve the spike glycoprotein sequences of 7 coronaviruses (HCoV-NL63, HCoV-229E, HCoV-OC43, HKU-1, MERS-CoV, SARS-CoV and SARS-CoV-2) which have previously infected the human population. In addition, spike glycoprotein sequences of different strains of SARS-CoV-2, isolated from 19 different countries (China, Japan, USA, Australia, Finland, Sweden, India, Colombia, Taiwan, Pakistan, Italy, Israel, Iran, Iran, Vietnam, Peru, Brazil, Spain, Nepal and

South Korea) around the globe were also retrieved from the VIPR database. Two phylogeny trees were constructed and for both the trees, the MUSCLE tool [72] was used in order to align the glycoprotein sequences and the alignment file was used to construct the phylogenetic trees with default parameters and 1000 bootstrap replicates, using the Neighbour Joining algorithm of MEGA 7.0.14 [73]

## T cell epitope prediction

*CTL epitope prediction* - 9-mer long CTL epitopes were predicted using NetCTL 1.2 server (<http://www.cbs.dtu.dk/services/NetCTL/>), recognized by the HLA Class I supertypes which are commonly occurring in human population, i.e., A1, A2, A3, A24, A26, B7, B8, B27, B39, B44, B58 and B62 [74]. In the NetCTL 1.2 server, the thresholds were set at 0.15, 0.05 and 0.75 for distinctive parameters such as proteasomal C-terminal cleavage, Transporter Associated with Antigen Processing (TAP) and epitope recognition, respectively. NetCTL supports epitope prediction with 54-89 % sensitivity and 94-99% specificity. Also, the epitopes recognized by other HLA Class I alleles were detected by Immune Epitope Consensus (IEDB) tool (<http://tools.iedb.org/mhci/>) [75].

*HTL epitope prediction* - 15-mer long HTL epitopes were predicted using NetMHCII pan 3.2 server ([www.cbs.dtu.dk/services/NetMHCIIpan/](http://www.cbs.dtu.dk/services/NetMHCIIpan/)), which had an affinity to class II HLA alleles [76]. The predicted peptides were classified as strong, intermediate and non-binders with threshold value set at 2, 10 and >10% respectively, based on the idea of percentile rank as given by NetMHCII pan 3.2 server.

The epitopes were screened on the basis of antigenicity as well as immunogenicity as predicted by VaxiJen v2.0 and IEDB class I immunogenicity web servers, respectively [77, 78]. The 3D structure of the spike glycoprotein was modelled using I-TASSER in order to visualize the selected epitopes on the protein surface [79-81].

## B cell epitope prediction

The ElliPro tool (<http://tools.iedb.org/ellipro/>) from IEDB server was used for predicting linear and conformational/discontinuous B cell epitopes with default parameters [82].

*IFN- $\gamma$  epitope prediction*- For both humoral and innate immunity, IFN- $\gamma$  plays important role in antiviral, anti-tumour and immune regulatory activities. Hence, IFN- $\gamma$  inducing epitopes are important for designing a potential multi-epitope vaccine. From the target protein, IFNepitope server (<http://crdd.osdd.net/raghava/ifnepitope/>) was used to predict out the IFN- $\gamma$  epitopes [83]. The server has a maximum accuracy of 81.39% and various approaches such as machine learning strategy, motive-based analysis and accuracy hybrid approach is used for the prediction of the epitopes.

## Population coverage

The IEDB population coverage analysis tool (<http://tools.iedb.org/population/>) was used in order to check if the epitopes of the designed vaccine had effectively covered the entire world population [84]. As, SARS-CoV-2 is a global pandemic the population coverage was checked for the total world population, United States, Europe,

China, South Asia and Oceania. The default parameters were used and the coverage was checked against the HLA class I and HLA class II binding alleles.

## **Multi epitope vaccine construct, Structural Modelling and Validation**

The screened CTL, HTL and IFN- $\gamma$  inducing epitopes from the target glycoprotein were together linked by glycine-proline rich GPGPG linkers. In addition, Cholera Toxin B (CTB) adjuvant was added by EAAAK linker to the N-terminal of the vaccine construct as it can induce regulatory immune responses. trRosetta was used to generate the 3D model of linear vaccine construct [85]. The tertiary structure was validated using ERRAT score [86] followed by ProSA-web analysis [22]. ProSA-web validates the structure based on Z-score predicted. Further, the overall quality of the generated model of vaccine was determined by Ramachandran plot analysis using RAMPAGE server [87].

## **Physicochemical properties of the vaccine construct-**

VaxiJen v2.0 [77] was used to check the antigenicity of the vaccine construct with a threshold value of 0.4. Viral databases were used to extract whole-protein antigenicity prediction models. Each set was made up of 100 identified antigens, and 100 non-antigens. The generated models were evaluated using data sets, utilizing internal leave-one-out cross-validation and external validation. The models implemented in the server worked well in both validations showing 70% to 89% predictive accuracy. Also, the allergenicity of the vaccine was checked using AllerTOP server [53]. This server employs auto-cross-covariance (ACC) grouping of protein sequences into uniform equal-length vectors. This has been applied to peptide study with the various types with quantitative structure-activity relationships (QSAR). The K-nearest neighbour algorithm (kNN, k=1) is used by the server to identify proteins based on a training set composed of 2427 identified allergens and 2427 non-allergens of various species. In addition, the allergenicity of the designed vaccine was cross checked by AllergenFP server (<http://ddg-pharmfac.net/AllergenFP/>) [54]. Other physicochemical properties like Isoelectric point, molecular weight, instability index, aliphatic index, half-life and GRAVY score of the vaccine was assessed using ExpPASy ProtParam server [55]. The vaccine construct was also checked for the presence of any signal peptides and transmembrane helices by SignalP4.1 (<http://www.cbs.dtu.dk/services/SignalP/>) [88] and TMHMM server v2.0 (<http://www.cbs.dtu.dk/services/TMHMM/>) [89], respectively.

## **Docking with TLR4 dimer, TLR2, MHC class I receptor and MHC class II receptor**

For generation of a stable immune response, it is essential for the vaccine to interact with target immune cell receptors. To study such interactions, molecular docking studies are performed. In this study, interactions of the vaccine with TLR4 dimer and TLR2 are studied as they localize on cell surface thereby inducing immune response when activated by the vaccine [90, 91]. In addition, the vaccine was also docked with MHC class I and MHC class II receptors. TLR4 hetero-tetramer structure and TLR2 structure were obtained from Protein Data Bank

ID 3FXI and ID 2Z7X, respectively whereas, the MHC class I and MHC class II receptors were obtained from PDB ID 1I1Y and 1KG0, respectively.

CPORT [92] was utilized for predicting the active and passive residues for the interactions. The docking of the vaccine with TLR4, TLR2, MHC class I and MHC class II receptors were performed by HADDOCK 2.4 (<http://www.bonvinlab.org/software/haddock2.4/>) [93]. The best cluster was chosen from the docked clusters based on lowest HADDOCK score.

HADDOCK Refinement Interface was used to refine the chosen cluster. The best structure after refinement from each docked complexes were chosen and their binding affinity was calculated using PRODIGY web server [94, 95]. Finally, the interacting residues between the vaccine and the TLRs were mapped using PDBsum (<http://www.ebi.ac.uk/thornton-srv/databases/pdbsum/Generate.html>) [96].

## Energy minimization and Molecular Dynamics Simulation

GROMACS (GRONingen MACHine for Chemical Simulations), a Linux-based program was used for the Molecular Dynamics Simulation (MDS) and energy minimisation [97]. MDS was done for the vaccine structure in order to see how it behaves in the *in vivo* biological system. OPLS-AA (Optimized Potential for Liquid Simulation-All Atom) force field constrain was used to generate the topology file required for energy minimization and equilibration. An equilibrated three-point water model, spc216 was used as the solvent to simulate the vaccine with periodic boundary conditions. The net charge of the vaccine construct was evaluated, and charged ions were added in order to neutralize the system. The simulation run was performed for 10ns of the energy minimised structure in order to find the Root Mean Square Deviation (RMSD) of backbone and Root Mean Square Fluctuation (RMSF) of side chain. The graphs were visualized using Xmgrace plotting tool [98].

## Reverse translation, codon optimization and *in silico* cloning of the vaccine

The Java Codon Adaptation Tool (JCat) (<http://www.jcat.de/>) was used for codon optimization and reverse translation which generated the cDNA sequence of the vaccine [99]. The codon optimized cDNA of the vaccine was then expressed in *E. coli* K-12 strain. The result consists of GC content and codon adaptation index (CAI) score, that can be used to access protein expression levels. In addition, the optimized multi-epitope vaccine sequence was inserted into the pET-28a (+) vector by SnapGene tool

## Immune simulation

C-IMMSIM server (<http://kraken.iac.rm.cnr.it/C-IMMSIM/>) was used for performing the immune simulation of the vaccine, in order to characterize the immune response profile and immunogenicity of the chimeric peptides [100]. C-ImmSim is an agent-based model that uses position-specific scoring matrices (PSSM) for immune response prediction using machine learning techniques for predicting immune interactions. The minimum recommended time between dose 1 and dose 2 for most of the vaccines currently in use, is 4 weeks [101]. The entire simulation ran for 1400 time steps which are about 15 months (a time step is about 8 hours). Two peptide injections were



given four weeks apart at time step 10, 94, 178, 262, 346, 430, 514, 598, 682, 766, 850, 934. Then a live virus was injected at time step 1100, which is about 12 months after the simulation starts.

## Conclusion

The current global pandemic of COVID-19 caused by SARS-CoV-2 is to date uncontrollable with high death rate. No proper medical preventives like vaccines are given to the patients yet for recovery. Application of *in silico* methods can be used to design an effective vaccine in lesser time and low cost. In this study, immunoinformatic tools are used for constructing a multi-epitope vaccine against SARS-CoV-2 consisting of CTL, HTL and IFN- $\gamma$  epitopes that can trigger strong immune responses. The designed multi-epitope vaccine was found to be both antigenic and immunogenic. The stability of the designed vaccine was assured by Molecular Dynamics Simulation and a stable interaction of the vaccine with immune receptors was confirmed by Molecular Docking studies. Further, *in silico* expression studies confirmed the vaccine's expression in bacterial host and the efficiency of the vaccine to trigger an immune response was validated by Immune Simulation studies.

## Declarations

**Acknowledgements:** The authors thank Dr. Joseph V.G., Chancellor Garden City University for his constant support to carry out this research work.

**Author contributions:** T.K., designed and performed experiments and helped in the writing, U.N., performed molecular dynamics simulation experiment, phylogenetic analysis and helped in the writing, S.B., designed and performed epitope selection prediction experiment, and helped in the writing, D.D., performed the docking and binding affinity experiments, helped in the writing, F.C., performed immune simulation experiment and helped in writing and D.M.M helped in data analysis and writing, and A.P.S. devised and supervised experiments, analyzed data, and helped in writing the manuscript.

**Competing Financial Interests:** There are no competing financial interests.

**Funding:** The authors received no external funding for this research.

**Correspondence:** Correspondence and requests for materials should be addressed to Anurag

1. Srivastava, [anurag.srivastava@gardencity.university](mailto:anurag.srivastava@gardencity.university), [anuiitkgp@gmail.com](mailto:anuiitkgp@gmail.com)

## References

1. Hui, D. S. *et al.* The continuing 2019-nCoV epidemic threat of novel coronaviruses to global health—The latest 2019 novel coronavirus outbreak in Wuhan, China. *International Journal of Infectious Diseases* **91**, 264 (2020).
2. Choudhary, S., Malik, Y. S., Tomar, S. & Tomar, S. (ChemRxiv, 2020). doi.org/10.26434/chemrxiv.12005988.v2
3. de Wit, E., van Doremalen, N., Falzarano, D. & Munster, V. J. SARS and MERS: recent insights into emerging coronaviruses. *Nature Reviews Microbiology* **14**, 523 (2016).
4. Ziebuhr, J. Current topics in microbiology and immunology. *Curr Top Microbiol Immunol* **287**, 57-94 (2005).

5. Anand, K., Ziebuhr, J., Wadhwani, P., Mesters, J. R. & Hilgenfeld, R. Coronavirus main proteinase (3CLpro) structure: basis for design of anti-SARS drugs. *Science* **300**, 1763-1767 (2003).
6. Su, S. *et al.* Epidemiology, genetic recombination, and pathogenesis of *Trends in microbiology* **24**, 490-502 (2016).
7. de Haan, C. A., Smeets, M., Vernooij, F., Vennema, H. & Rottier, P. Mapping of the coronavirus membrane protein domains involved in interaction with the spike *Journal of virology* **73**, 7441-7452 (1999).
8. Weiss, S. R. & Navas-Martin, S. Coronavirus pathogenesis and the emerging pathogen severe acute respiratory syndrome coronavirus. *Mol. Biol. Rev.* **69**, 635-664 (2005).
9. Nicholson, K. G., Kent, J. & Ireland, D. C. Respiratory viruses and exacerbations of asthma in adults. *Bmj* **307**, 982-986 (1993).
10. Bergmann, C. C., Lane, T. E. & Stohlman, S. A. Coronavirus infection of the central nervous system: host-virus stand-off. *Nature Reviews Microbiology* **4**, 121-132 (2006).
11. Perlman, S. & Netland, J. Coronaviruses post-SARS: update on replication and pathogenesis. *Nature reviews microbiology* **7**, 439-450 (2009).
12. Lu, R. *et al.* Genomic characterisation and epidemiology of 2019 novel coronavirus: implications for virus origins and receptor binding. *The Lancet* **395**, 565-574 (2020).
13. Hoffmann, M. *et al.* SARS-CoV-2 cell entry depends on ACE2 and TMPRSS2 and is blocked by a clinically proven protease inhibitor. *Cell* (2020).
14. Wong, S. K., Li, , Moore, M. J., Choe, H. & Farzan, M. A 193-amino acid fragment of the SARS coronavirus S protein efficiently binds angiotensin-converting enzyme 2. *J Biol Chem* **279**, 3197-3201, doi:10.1074/jbc.C300520200 (2004).
15. Bonavia, A., Zelus, D., Wentworth, D. E., Talbot, P. J. & Holmes, K. V. Identification of a receptor-binding domain of the spike glycoprotein of human coronavirus HCoV-229E. *Journal of Virology* **77**, 2530-2538 (2003).
16. Chan, J. F.-W. *et al.* Genomic characterization of the 2019 novel human-pathogenic coronavirus isolated from a patient with atypical pneumonia after visiting Wuhan. *Emerging Microbes & Infections* **9**, 221-236 (2020).
17. Malik, Y. S. *et al.* Emerging novel coronavirus (2019-nCoV)—current scenario, evolutionary perspective based on genome analysis and recent developments. *Veterinary Quarterly* **40**, 68-76 (2020).
18. Chauhan, V., Rungta, T., Goyal, & Singh, M. P. Designing a multi-epitope based vaccine to combat Kaposi Sarcoma utilizing immunoinformatics approach. *Scientific reports* **9**, 1-15 (2019).
19. Faisal, A.-R. M., Imtiaz, S. H., Zerin, , Rahman, T. & Shekhar, H. U. Computer aided epitope design as a peptide vaccine component against Lassa virus. *Bioinformatics* **13**, 417 (2017).
20. Dorosti, H. *et al.* Vaccinomics approach for developing multi-epitope peptide pneumococcal vaccine. *Journal of Biomolecular Structure and Dynamics* **37**, 3524- 3535 (2019).
21. Atapour, A. *et al.* Designing a fusion protein vaccine against HCV: an in silico approach. *International Journal of Peptide Research and Therapeutics* **25**, 861-872 (2019).
22. Wiederstein, M. & Sippl, J. ProSA-web: interactive web service for the recognition of errors in three-dimensional structures of proteins. *Nucleic acids research* **35**, W407- W410 (2007).
23. Morse, J. S., Lalonde, T., Xu, S. & Liu, R. Learning from the Past: Possible Urgent Prevention and Treatment Options for Severe Acute Respiratory Infections Caused by 2019-nCoV. *ChemBiochem* **21**, 730-738 (2020).

24. de Oliveira Tosta, S. F. *et al.* Multi-epitope based vaccine against Yellow fever virus applying immunoinformatics approaches. *Journal of Biomolecular Structure and Dynamics*, 1-28 (2019).
25. Srivastava, S. *et al.* Design of novel multi-epitope vaccines against severe acute respiratory syndrome validated through multistage molecular interaction and dynamics. *Journal of Biomolecular Structure and Dynamics* **37**, 4345-4360 (2019).
26. Goodman, A. G. *et al.* A human multi-epitope recombinant vaccinia virus as a universal T cell vaccine candidate against influenza virus. *PLoS one* **6** (2011).
27. Nosrati, M., Behbahani, M. & Mohabatkar, H. Towards the first multi-epitope recombinant vaccine against Crimean-Congo hemorrhagic fever virus: A computer- aided vaccine design approach. *Journal of biomedical informatics* **93**, 103160 (2019).
28. Zhang, L. Multi-epitope vaccines: a promising strategy against tumors and viral infections. *Cellular & molecular immunology* **15**, 182-184 (2018).
29. Sbai, , Mehta, A. & DeGroot, A. Use of T cell epitopes for vaccine development. *Current drug targets-Infectious disorders* **1**, 303-313 (2001).
30. Sette, A. & Fikes, J. Epitope-based vaccines: an update on epitope identification, vaccine design and delivery. *Current opinion in immunology* **15**, 461-470 (2003).
31. Jabbar, B. *et al.* Antigenic Peptide Prediction From E6 and E7 Oncoproteins of HPV Types 16 and 18 for Therapeutic Vaccine Design Using Immunoinformatics and MD Simulation Analysis. *Frontiers in immunology* **9**, 3000 (2018).
32. Mirza, M. U. *et al.* Towards peptide vaccines against Zika virus: Immunoinformatics combined with molecular dynamics simulations to predict antigenic epitopes of Zika viral proteins. *Scientific reports* **6**, 37313 (2016).
33. Shahid, F., Ashfaq, U. A., Javaid, A. & Khalid, H. Immunoinformatics guided rational design of a next generation multi epitope based peptide (MEBP) vaccine by exploring Zika virus proteome. *Infection, Genetics and Evolution* **80**, 104199 (2020).
34. Yin, D. *et al.* A novel multi-epitope recombined protein for diagnosis of human brucellosis. *BMC infectious diseases* **16**, 219 (2016).
35. Lu, C. *et al.* A novel multi- epitope vaccine from MMSA- 1 and DKK 1 for multiple myeloma immunotherapy. *British journal of haematology* **178**, 413-426 (2017).
36. He, R. *et al.* Efficient control of chronic LCMV infection by a CD4 T cell epitope- based heterologous prime-boost vaccination in a murine *Cellular & molecular immunology* **15**, 815-826 (2018).
37. Saadi, M., Karkhah, A. & Nouri, H. R. Development of a multi-epitope peptide vaccine inducing robust T cell responses against brucellosis using immunoinformatics based approaches. *Infection, Genetics and Evolution* **51**, 227-234 (2017).
38. Lu, I.-N., Farinelle, S., Sausy, & Muller, C. P. Identification of a CD4 T-cell epitope in the hemagglutinin stalk domain of pandemic H1N1 influenza virus and its antigen-driven TCR usage signature in BALB/c mice. *Cellular & molecular immunology* **14**, 511-520 (2017).
39. Jiang, P. *et al.* Evaluation of tandem Chlamydia trachomatis MOMP multi-epitopes vaccine in BALB/c mice *Vaccine* **35**, 3096-3103 (2017).

40. Lennerz, V. *et al.* Immunologic response to the survivin-derived multi-epitope vaccine EMD640744 in patients with advanced solid tumors. *Cancer immunology, immunotherapy* **63**, 381-394 (2014).
41. Zhu, S. *et al.* Hepatitis B virus surface antigen as delivery vector can enhance Chlamydia trachomatis MOMP multi-epitope immune response in mice. *Applied microbiology and biotechnology* **98**, 4107-4117 (2014).
42. Mahmoodi, S. *et al.* Harnessing bioinformatics for designing a novel multiepitope peptide vaccine against breast cancer. *Current pharmaceutical biotechnology* **17**, 1100-1114 (2016).
43. Davies, M. N. & Flower, D. R. Harnessing bioinformatics to discover new *Drug discovery today* **12**, 389-395 (2007).
44. Guo, L. *et al.* Immunological features and efficacy of a multi-epitope vaccine CTB-UE against H. pylori in BALB/c mice *Applied microbiology and biotechnology* **98**, 3495-3507 (2014).
45. Zhou, W.-Y. *et al.* Therapeutic efficacy of a multi-epitope vaccine against Helicobacter pylori infection in BALB/c mice model. *Vaccine* **27**, 5013-5019 (2009).
46. Cao, Y. *et al.* Rational design and efficacy of a multi-epitope recombinant protein vaccine against foot-and-mouth disease virus serotype A in pigs. *Antiviral research* **140**, 133-141 (2017).
47. Slingluff, C. *et al.* A randomized phase II trial of multiepitope vaccination with melanoma peptides for cytotoxic T cells and helper T cells for patients with metastatic melanoma (E1602). *Clinical Cancer Research* **19**, 4228-4238 (2013).
48. Toledo, H. *et al.* A phase I clinical trial of a multi-epitope polypeptide TAB9 combined with Montanide ISA 720 adjuvant in non-HIV-1 infected human volunteers. *Vaccine* **19**, 4328-4336 (2001).
49. Tamura, S.-i., Funato, H., Nagamine, T., Aizawa, C. & Kurata, T. Effectiveness of cholera toxin B subunit as an adjuvant for nasal influenza vaccination despite pre-existing immunity to CTB. *Vaccine* **7**, 503-505 (1989).
50. Kim, H. J., Kim, -K., Seo, S. B., Lee, H. J. & Kim, H.-J. Intranasal vaccination with peptides and cholera toxin subunit B as adjuvant to enhance mucosal and systemic immunity to respiratory syncytial virus. *Archives of pharmacal research* **30**, 366-371 (2007).
51. Hou, J. *et al.* Cholera toxin B subunit acts as a potent systemic adjuvant for HIV-1 DNA vaccination intramuscularly in mice. *Human vaccines & immunotherapeutics* **10**, 1274-1283 (2014).
52. Kavooosi, M., Creagh, A. L., Kilburn, D. G. & Haynes, C. A. Strategy for selecting and characterizing linker peptides for CBM9- tagged fusion proteins expressed in Escherichia coli. *Biotechnology and bioengineering* **98**, 599-610 (2007).
53. Dimitrov, I., Bangov, I., Flower, D. R. & Doytchinova, I. AllerTOP v. 2—a server for in silico prediction of allergens. *Journal of molecular modeling* **20**, 2278 (2014).
54. Dimitrov, I., Naneva, L., Doytchinova, I. & Bangov, AllergenFP: allergenicity prediction by descriptor fingerprints. *Bioinformatics* **30**, 846-851 (2014).
55. Walker, J. M. *The proteomics protocols handbook*. (Springer, 2005).
56. Rehman, H. M. *et al.* A Putative Prophylactic Solution for COVID-19: Development of Novel Multiepitope Vaccine Candidate against SARS- COV- 2 by Comprehensive Immunoinformatic and Molecular Modelling Approach. (2020). doi: 10.20944/preprints202003.0242.v1
57. ul Qamar, M. T. *et al.* Designing of a next generation multiepitope based vaccine (MEV) against SARS-COV-2: Immunoinformatics and in silico approaches. *BioRxiv* (2020). org/10.1101/2020.02.28.970343

58. Kyte, J. & Doolittle, R. F. A simple method for displaying the hydropathic character of a protein. *Journal of molecular biology* **157**, 105-132 (1982).
59. Ikai, A. Thermostability and aliphatic index of globular proteins. *The Journal of Biochemistry* **88**, 1895-1898 (1980).
60. Boehme, K. W. & Compton, T. Innate sensing of viruses by toll-like *Journal of virology* **78**, 7867-7873 (2004).
61. Xagorari, A. & Chlichlia, K. Toll-like receptors and viruses: induction of innate antiviral immune responses. *The open microbiology journal* **2**, 49 (2008).
62. Carty, M. & Bowie, A. G. Recent insights into the role of Toll- like receptors in viral infection. *Clinical & Experimental Immunology* **161**, 397-406 (2010).
63. Vaure, C. & Liu, A comparative review of toll-like receptor 4 expression and functionality in different animal species. *Frontiers in immunology* **5**, 316 (2014).
64. Phongsisay, V., Iizasa, E. i., Hara, H. & Yoshida, H. Evidence for TLR4 and FcRγ- CARD9 activation by cholera toxin B subunit and its direct bindings to TREM2 and LMIR5 receptors. *Molecular immunology* **66**, 463-471 (2015).
65. Solanki, V., Tiwari, & Tiwari, V. Prioritization of potential vaccine targets using comparative proteomics and designing of the chimeric multi-epitope vaccine against *Pseudomonas aeruginosa*. *Scientific reports* **9**, 1-19 (2019).
66. Dar, H. A. *et al.* Immunoinformatics-Aided Design and Evaluation of a Potential Multi-Epitope Vaccine against *Klebsiella Pneumoniae*. *Vaccines* **7**, 88 (2019).
67. Ali, M. *et al.* Exploring dengue genome to construct a multi-epitope based subunit vaccine by utilizing immunoinformatics approach to battle against dengue *Sci Rep* **7**, 9232 (2017).
68. Ojha, R., Pareek, A., Pandey, R. K., Prusty, D. & Prajapati, V. K. Strategic Development of a Next-Generation Multi-Epitope Vaccine To Prevent Nipah Virus Zoonotic Infection. *ACS omega* **4**, 13069-13079 (2019).
69. Kamthania, M. *et al.* Immunoinformatics Approach to Design T-cell Epitope-Based Vaccine Against Hendra Virus. *International Journal of Peptide Research and Therapeutics* **25**, 1627-1637 (2019).
70. Pandey, R. K., Bhatt, T. K. & Prajapati, V. K. Novel immunoinformatics approaches to design multi-epitope subunit vaccine for malaria by investigating anopheles salivary protein. *Scientific reports* **8**, 1-11 (2018).
71. Mishra, S. & Sinha, S. Immunoinformatics and modeling perspective of T cell epitope- based cancer immunotherapy: a holistic picture. *Journal of Biomolecular Structure and Dynamics* **27**, 293-305 (2009).
72. Edgar, R. C. MUSCLE: a multiple sequence alignment method with reduced time and space complexity. *BMC Bioinformatics* **5**, 113, doi:10.1186/1471-2105-5-113 (2004).
73. Kumar, S., Stecher, G. & Tamura, K. MEGA7: Molecular Evolutionary Genetics Analysis Version 7.0 for Bigger *Mol Biol Evol* **33**, 1870-1874, doi:10.1093/molbev/msw054 (2016)
74. Larsen, M. V. *et al.* Large-scale validation of methods for cytotoxic T-lymphocyte epitope prediction. *BMC bioinformatics* **8**, 424 (2007).
75. Moutaftsi, M. *et al.* A consensus epitope prediction approach identifies the breadth of murine T CD8+-cell responses to vaccinia virus. *Nature biotechnology* **24**, 817-819 (2006).
76. Jensen, K. K. *et al.* Improved methods for predicting peptide binding affinity to MHC class II molecules. *Immunology* **154**, 394-406 (2018).

77. Doytchinova, I. A. & Flower, D. R. VaxiJen: a server for prediction of protective antigens, tumour antigens and subunit vaccines. *BMC bioinformatics* **8**, 4 (2007).
78. Calis, J. J. *et al.* Properties of MHC class I presented peptides that enhance immunogenicity. *PLoS computational biology* **9** (2013).
79. Roy, A., Kucukural, A. & Zhang, Y. I-TASSER: a unified platform for automated protein structure and function prediction. *Nature protocols* **5**, 725 (2010).
80. Yang, J. *et al.* The I-TASSER Suite: protein structure and function prediction. *Nature methods* **12**, 7 (2015).
81. Yang, J. & Zhang, Y. I-TASSER server: new development for protein structure and function predictions. *Nucleic acids research* **43**, W174-W181 (2015).
82. Ponomarenko, J. *et al.* ElliPro: a new structure-based tool for the prediction of antibody epitopes. *BMC bioinformatics* **9**, 514 (2008).
83. Dhanda, S. K., Vir, & Raghava, G. P. Designing of interferon-gamma inducing MHC class-II binders. *Biology direct* **8**, 30 (2013).
84. Bui, H.-H. *et al.* Predicting population coverage of T-cell epitope-based diagnostics and vaccines. *BMC bioinformatics* **7**, 153 (2006).
85. Yang, J. *et al.* Improved protein structure prediction using predicted interresidue orientations. *Proceedings of the National Academy of Sciences* (2020).
86. Colovos, C. & Yeates, T. O. Verification of protein structures: patterns of nonbonded atomic interactions. *Protein science* **2**, 1511-1519 (1993).
87. Lovell, S. C. *et al.* Structure validation by C $\alpha$  geometry:  $\phi$ ,  $\psi$  and C $\beta$  *Proteins: Structure, Function, and Bioinformatics* **50**, 437-450 (2003).
88. Nielsen, H. in *Protein function prediction* 59-73 (Springer, 2017).
89. Krogh, A., Larsson, B., Von Heijne, G. & Sonnhammer, E. L. Predicting transmembrane protein topology with a hidden Markov model: application to complete genomes. *Journal of molecular biology* **305**, 567-580 (2001).
90. Patel, M. C. *et al.* Novel drugs targeting Toll-like receptors for antiviral *Future virology* **9**, 811-829 (2014).
91. Chen, J., Ng, M. M.-L. & Chu, J. J. Activation of TLR2 and TLR6 by dengue NS1 protein and its implications in the immunopathogenesis of dengue virus infection. *PLoS pathogens* **11** (2015).
92. de Vries, S. J. & Bonvin, A. M. CPORT: a consensus interface predictor and its performance in prediction-driven docking with HADDOCK. *PloS one* **6** (2011).
93. Van Zundert, G. *et al.* The HADDOCK2. 2 web server: user-friendly integrative modeling of biomolecular complexes. *Journal of molecular biology* **428**, 720-725 (2016).
94. Vangone, A. & Bonvin, A. M. Contacts-based prediction of binding affinity in protein–protein complexes. *elife* **4**, e07454 (2015).
95. Xue, L. C., Rodrigues, J. P., Kastritis, P. L., Bonvin, A. M. & Vangone, A. PRODIGY: a web server for predicting the binding affinity of protein–protein complexes. *Bioinformatics* **32**, 3676-3678 (2016).
96. Laskowski, R. A., Jabłońska, J., Pravda, L., Vařeková, R. S. & Thornton, J. M. PDBsum: Structural summaries of PDB entries. *Protein science* **27**, 129-134 (2018).
97. Abraham, M. J. *et al.* GROMACS: High performance molecular simulations through multi-level parallelism from laptops to supercomputers. *SoftwareX* **1**, 19-25 (2015).

98. Turner, P. XMGRACE, Version 5.1. 19. *Center for Coastal and Land-Margin Research, Oregon Graduate Institute of Science and Technology, Beaverton, OR* (2005).
99. Grote, A. *et al.* JCat: a novel tool to adapt codon usage of a target gene to its potential expression host. *Nucleic acids research* **33**, W526-W531 (2005).
100. Rapin, N., Lund, O., Bernaschi, M. & Castiglione, F. Computational immunology meets bioinformatics: the use of prediction tools for molecular binding in the simulation of the immune system. *PLoS One* **5** (2010).
101. Castiglione, F., Mantile, F., De Berardinis, P. & Prisco, A. How the interval between prime and boost injection affects the immune response in a computational model of the immune system. *Computational and mathematical methods in medicine* **2012** (2012).

## Figures

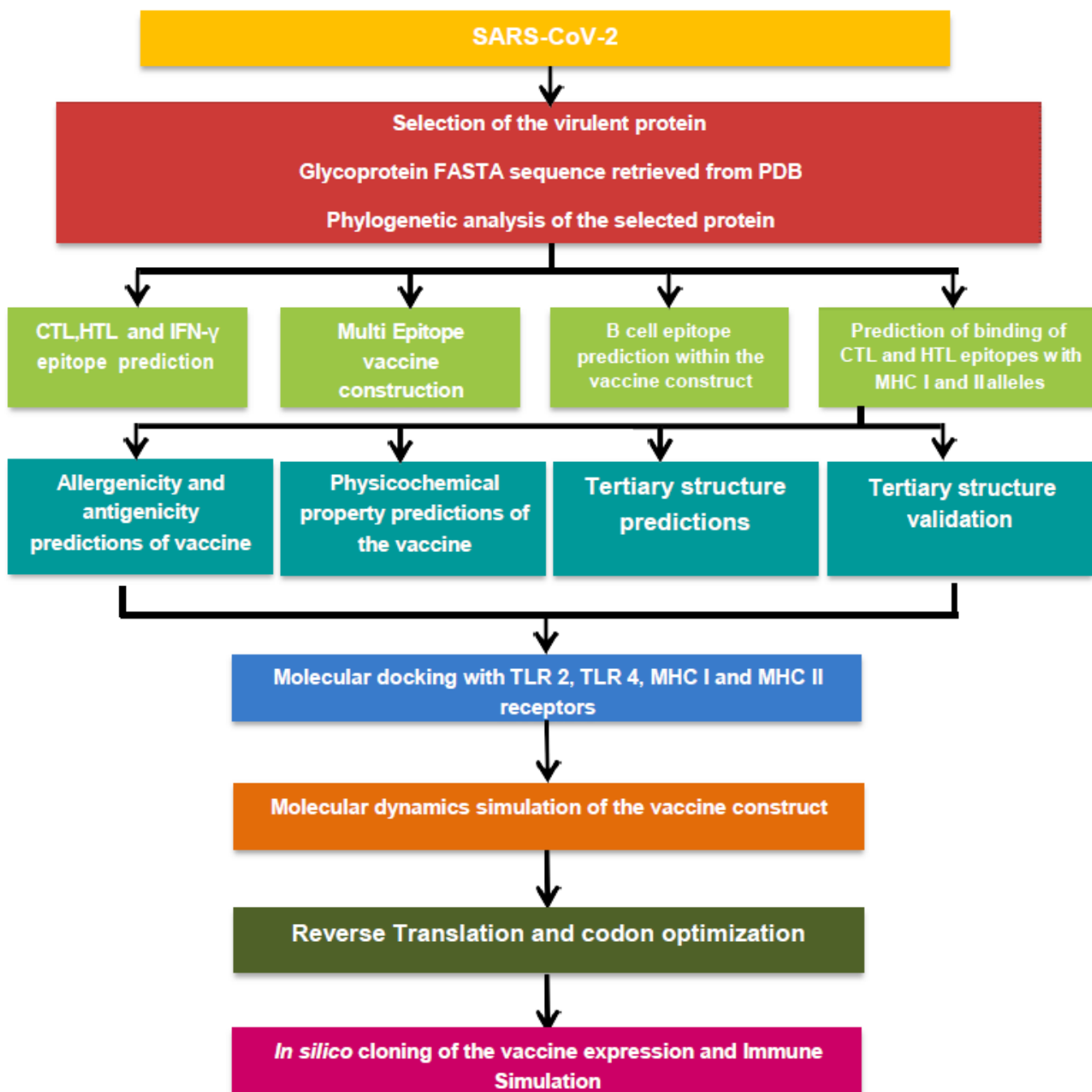


**Figure 1**

Flowchart for the designed study. The entire approach used in the study comprises of several phases, which involves identifying the target protein and its phylogenetic analysis. Epitope predictions from the chosen protein (CTI, HTL, IFN- $\gamma$  and B cell epitopes); vaccine construction and its quality check. Molecular Docking with immune cell receptor, followed by MDS to check vaccine's stability. Lastly, in silico vaccine expression and immune simulation to understand how the vaccine elicits an immune response.



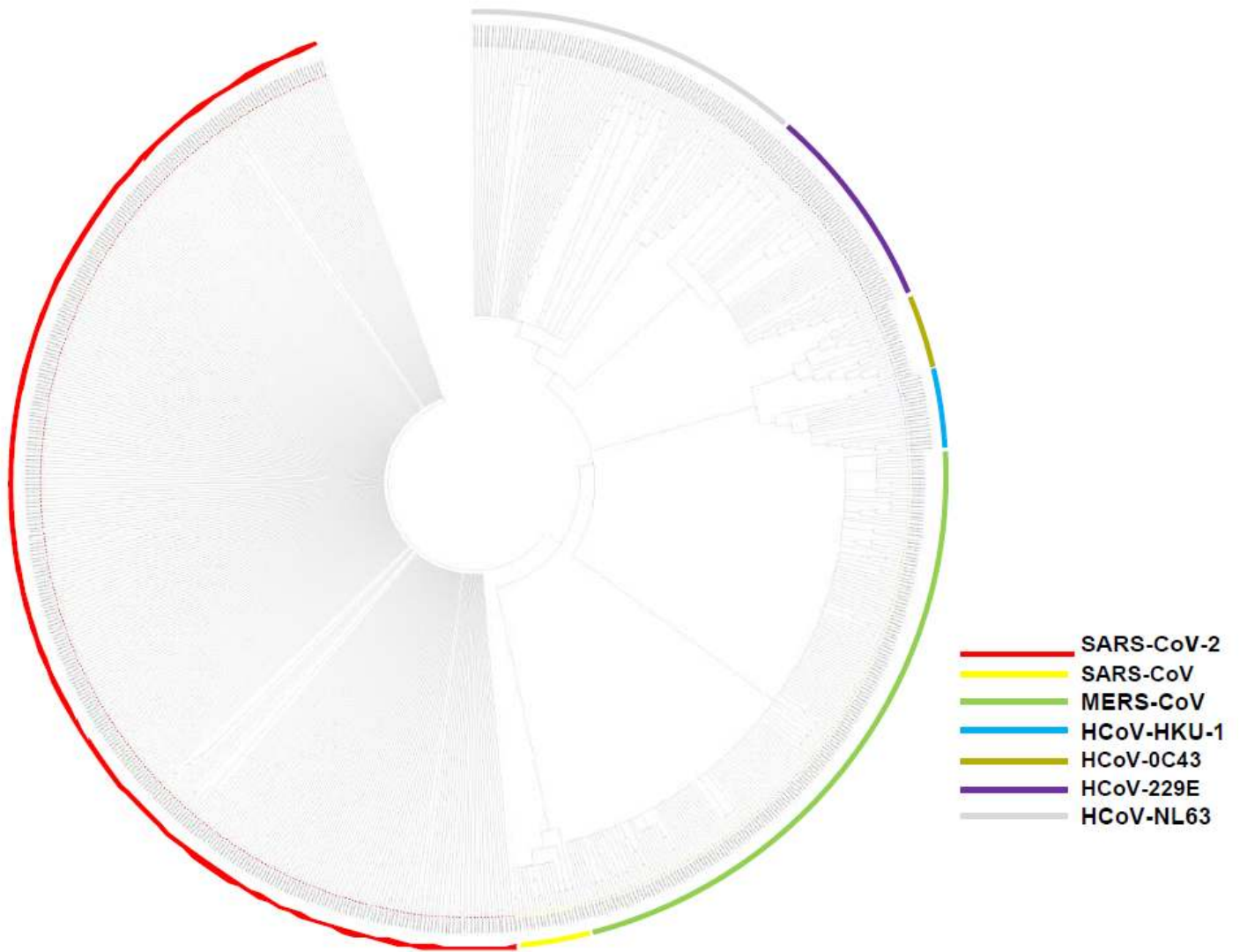


**Figure 2**

Phylogenetic analysis of spike glycoprotein of 7 coronaviruses (HCoV-NL63, HCoV-229E, HCoV-0C43, HKU-1, MERS-CoV, SARS-CoV and SARS-CoV-2) infecting humans. SARS-CoV-2 has shown very low rate of diversification.

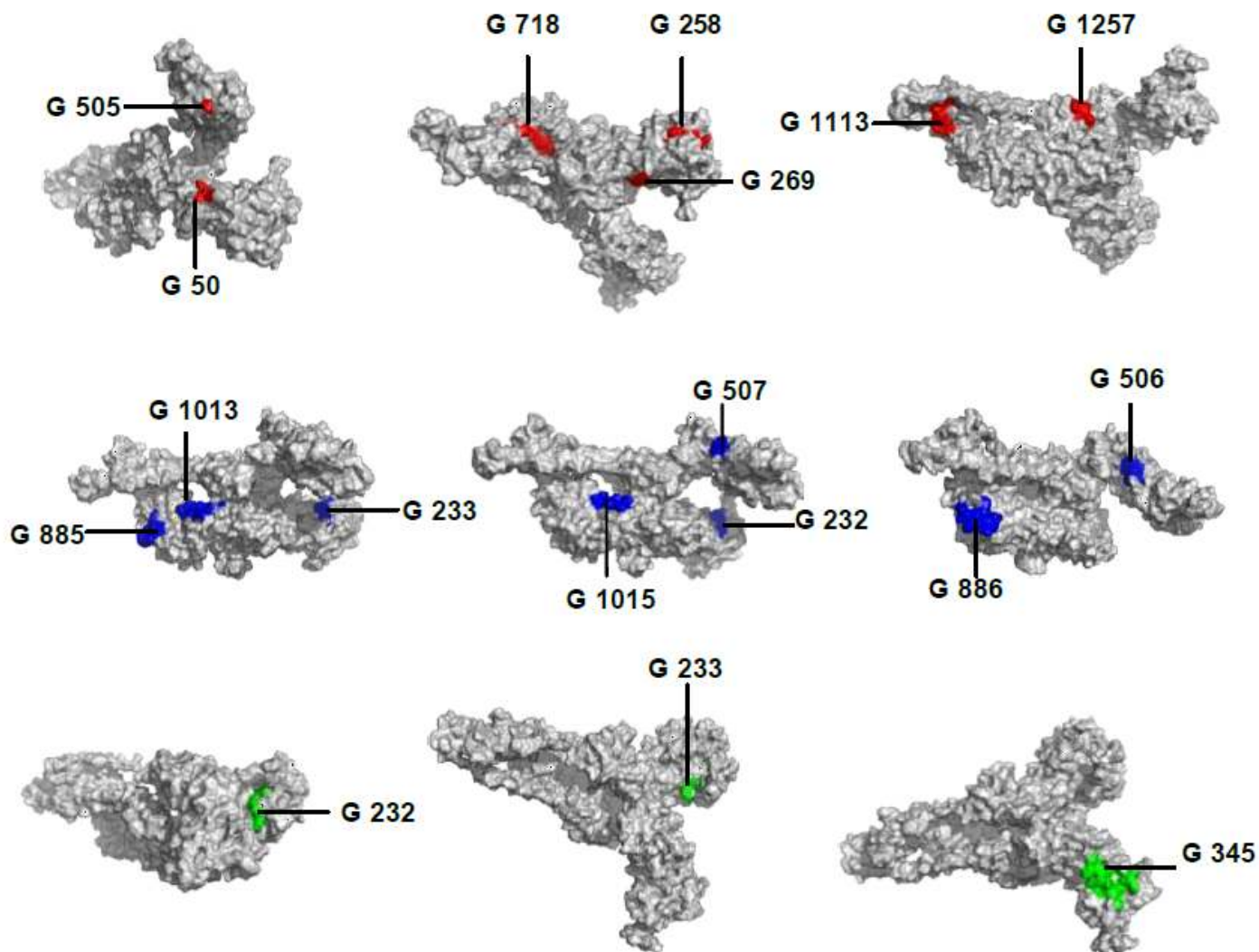


**Figure 3**

Tertiary structure of the spike protein with CTL epitopes marked by red colour, HTL epitopes are marked by blue colour and IFN- $\gamma$  epitopes marked by green colour, showing their surface positions.

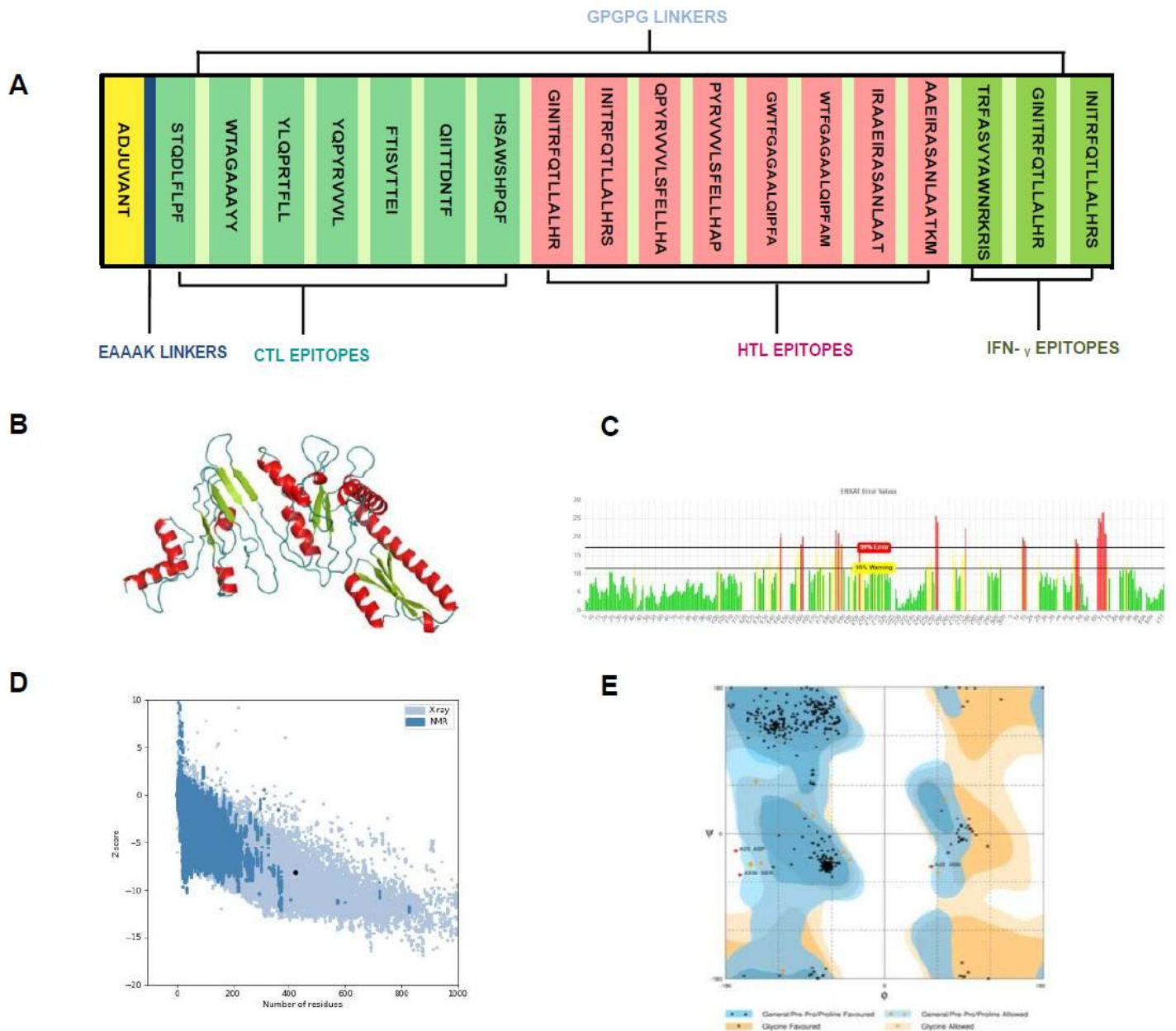


**Figure 4**

(A) Linear vaccine construct with CTL, HTL and IFN- $\gamma$  depicted in sea green, pink and green boxes, respectively. EAAAK linker (deep blue) was used for linking the adjuvant and GPGPG linkers (pale green) were used for linking the epitopes. (B) 3D model of the final vaccine construct. Red, Limon and Blue represent the helical, sheet and loop region, respectively. (C) Validation of the vaccine structure by ERRAT with a score of 74.2947. (D) Validation of the structure with a Z-score of -8.1 using ProSA. (E) Ramachandran plot analysing using RAMPAGE 96.4%, 2.9% and 0.7% in the favoured, allowed and outlier region, respectively.

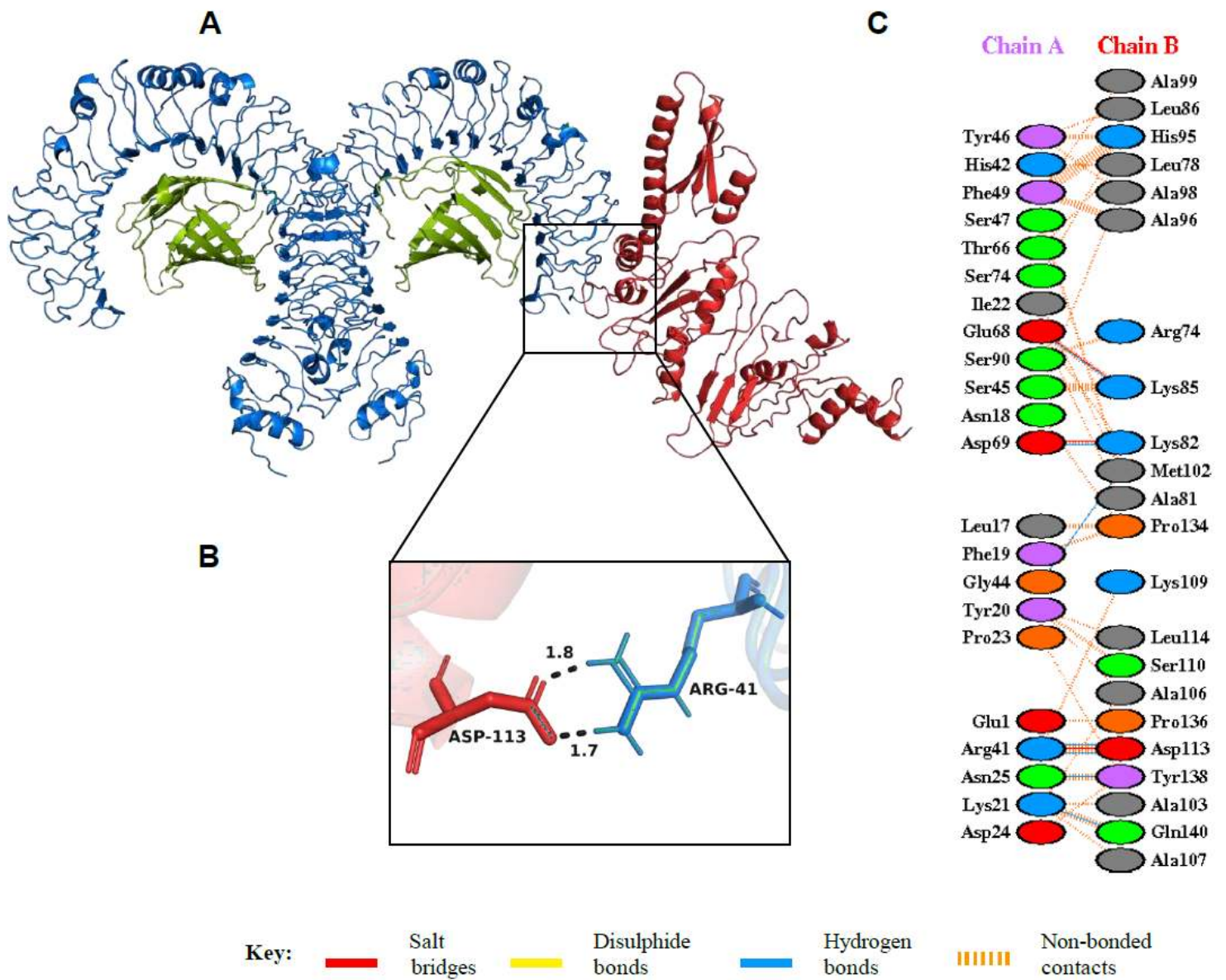


**Figure 5**

(A) Figure obtained after molecular docking, showing TLR4/MD2 tetramer-vaccine docked complex. Vaccine construct is shown in red colour while TLR4 dimer is shown in blue colour and MD2 co-receptor shown in green colour. (B) Interacting residues between docked TLR4/MD2 tetramer (chain A) and vaccine (chain B). (C) Few prominent hydrogen bonds within vaccine-TLR4 complex are focused.



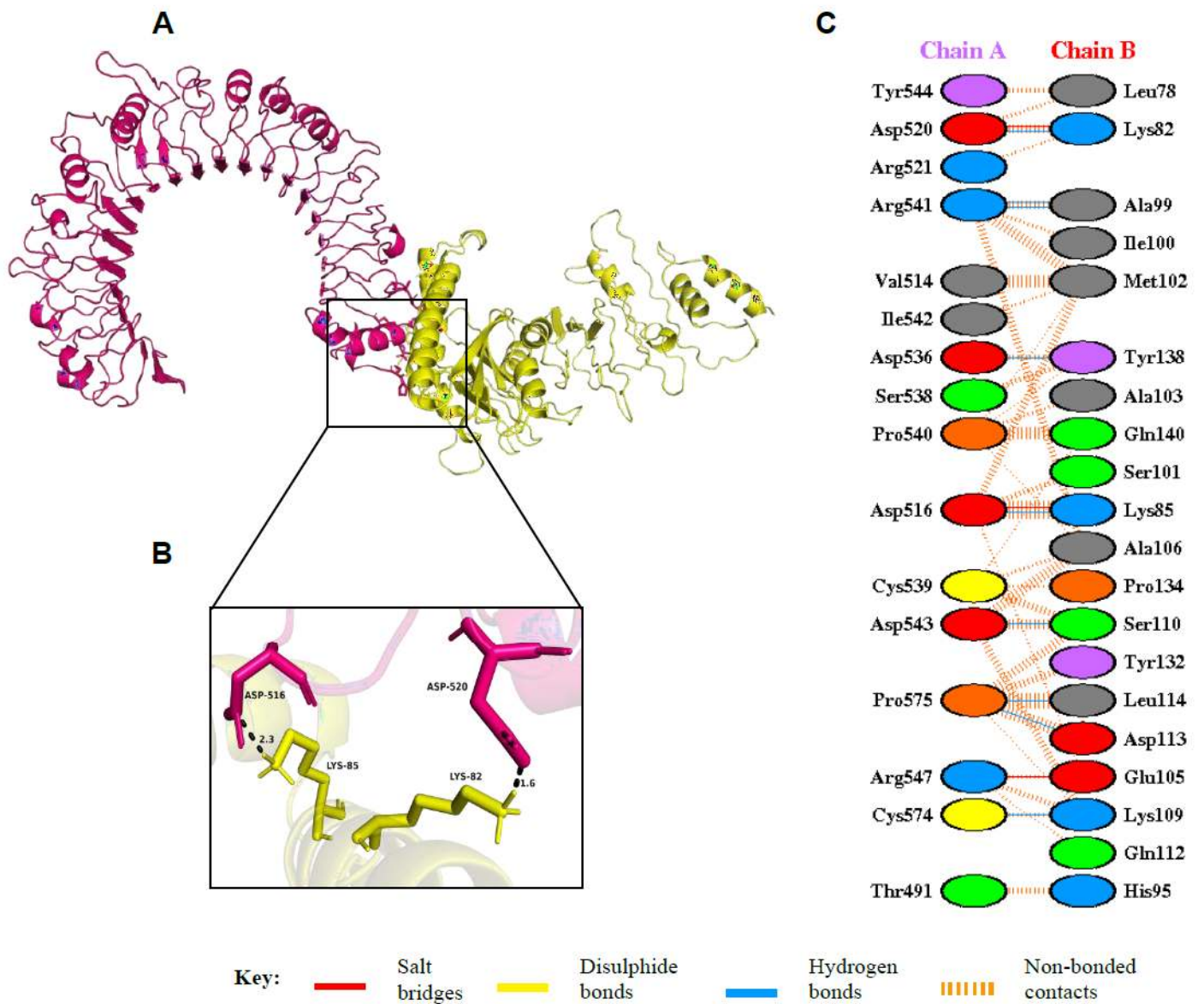


**Figure 6**

(A) Figure obtained after molecular docking, showing TLR2-vaccine docked complex. Vaccine construct is shown in yellow colour while TLR2 is shown in hot pink colour. (B) Interacting residues between docked TLR2 (chain A) and vaccine (chain B). (C) Few prominent hydrogen bonds within vaccine-TLR2 complex are focused.

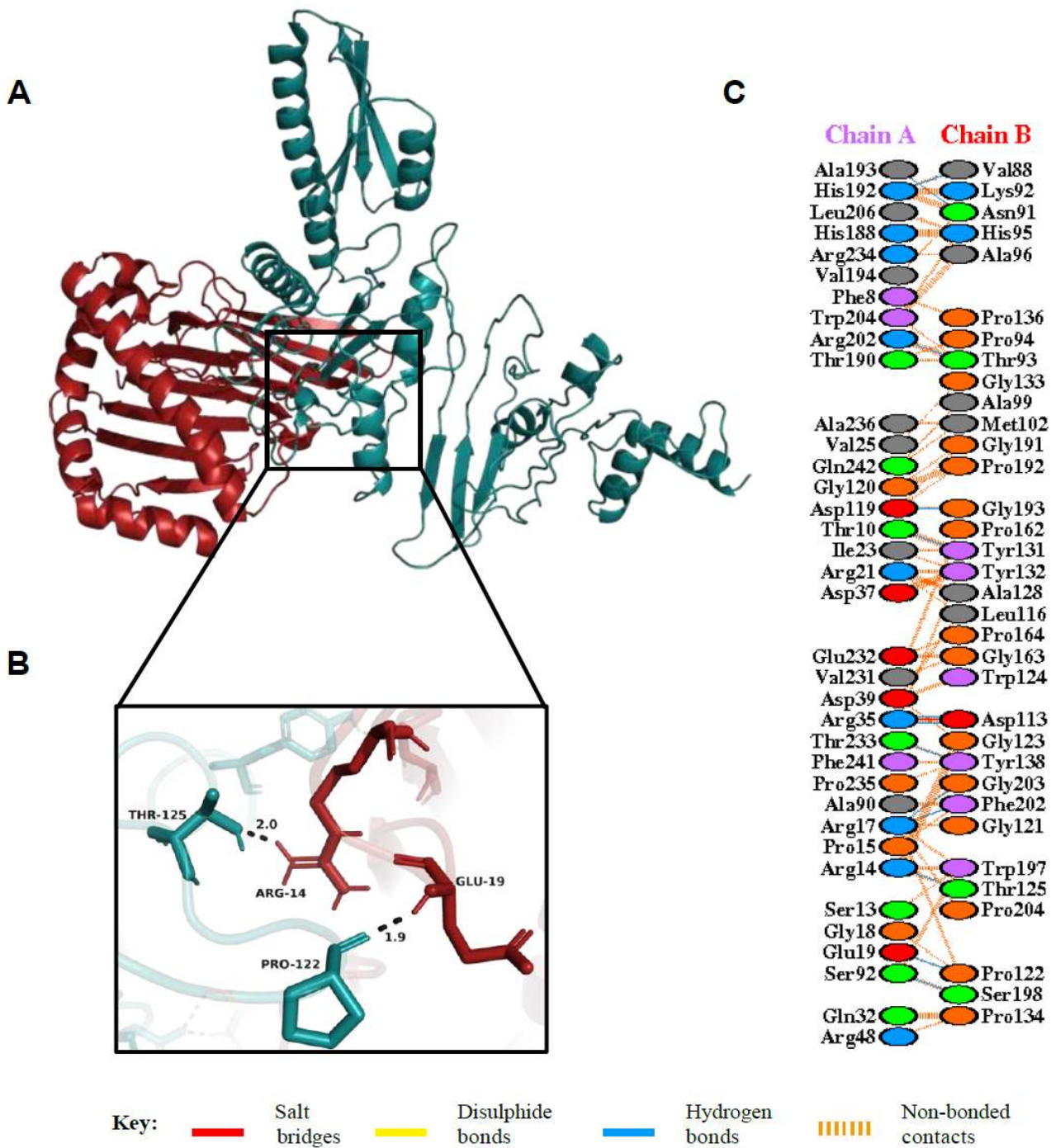


**Figure 7**

(A) Figure obtained after molecular docking, showing MHC I-vaccine docked complex. Vaccine construct is shown in deep teal colour while MHC I is shown in fire brick colour. (B) Interacting residues between docked MHC I (chain A) and vaccine (chain B). (C) Few prominent hydrogen bonds within vaccine-MHC I complex are focused.

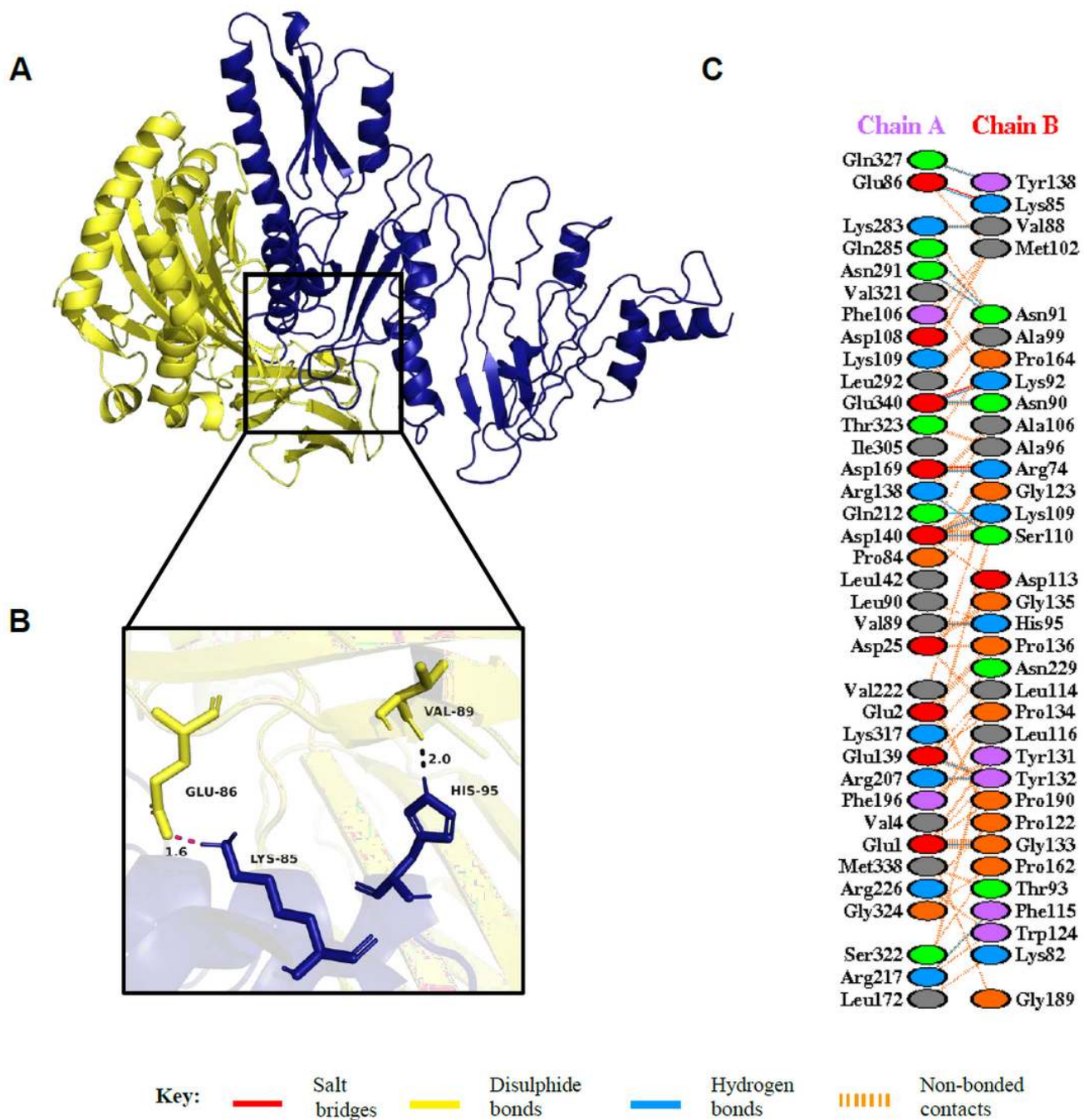
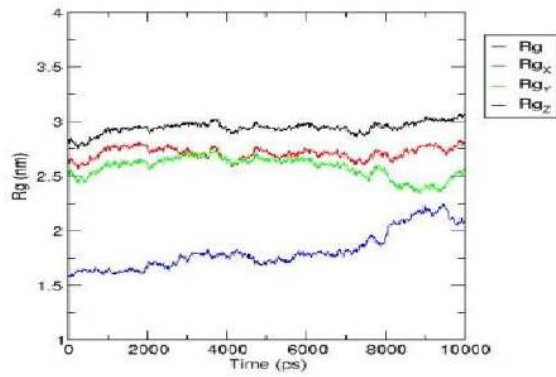


**Figure 8**

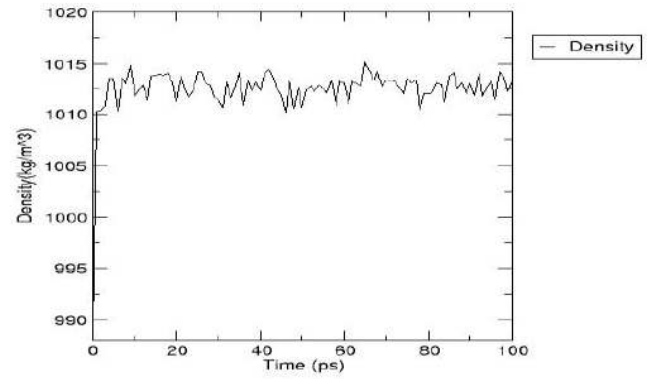
(A) Figure obtained after molecular docking, showing MHC II-vaccine docked complex. Vaccine construct is shown in blue colour while MHC II is shown in yellow colour. (B) Interacting residues between docked MHC II (chain A) and vaccine (chain B). (C) Few prominent hydrogen bonds within vaccine-MHC II complex are focused.



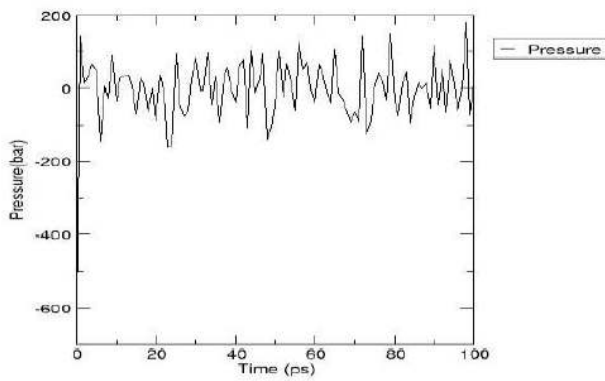
**A** Radius of gyration (total and around axes)



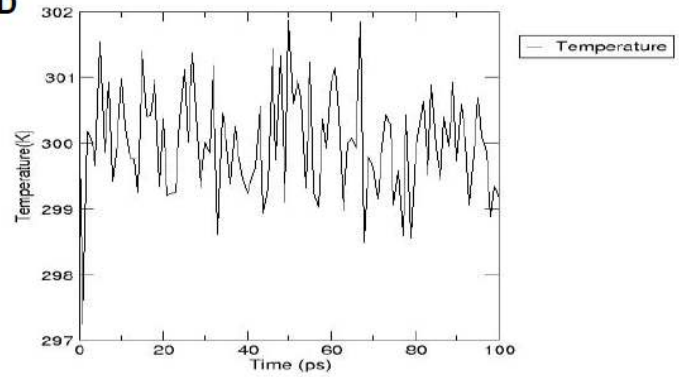
**B** GROMACS Energies



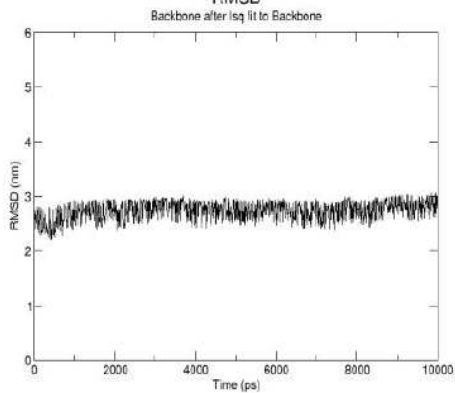
**C** GROMACS Energies



**D** GROMACS Energies



**E** RMSD



**F** RMS fluctuation

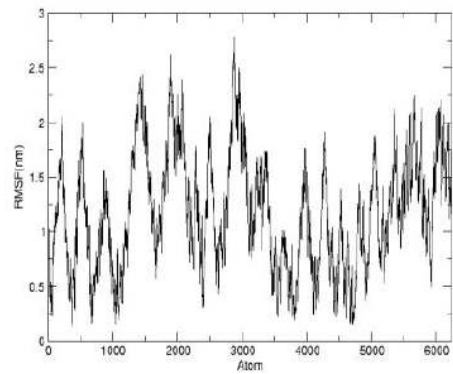


**Figure 9**

(A) Radius of Gyration plot showing compactness of the vaccine around its axes. (B) Graph showing density of the system during simulation. (C) Graph showing the pressure of the system during simulation. (D) Graph showing the equilibrated temperature during energy minimisation. (E) RMSD plot of the vaccine construct indicating stability. (F) RMSF plot of the vaccine construct showing high fluctuations, indicating high flexibility.



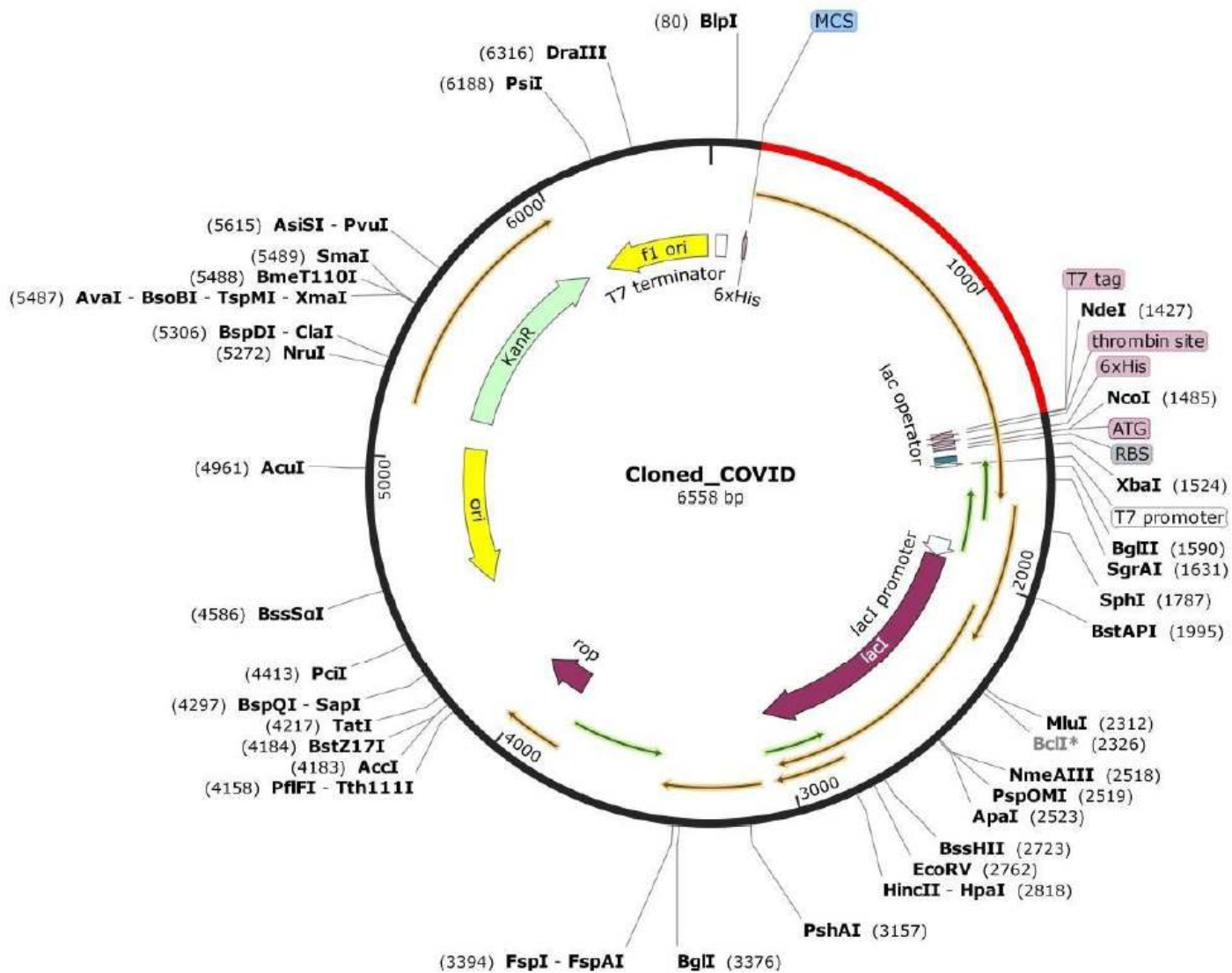


**Figure 10**

In silico restriction cloning. The red coloured portion represents the codon optimised multi-epitope vaccine inserted into the pET-28a (+) expression vector which is represented in black colour.

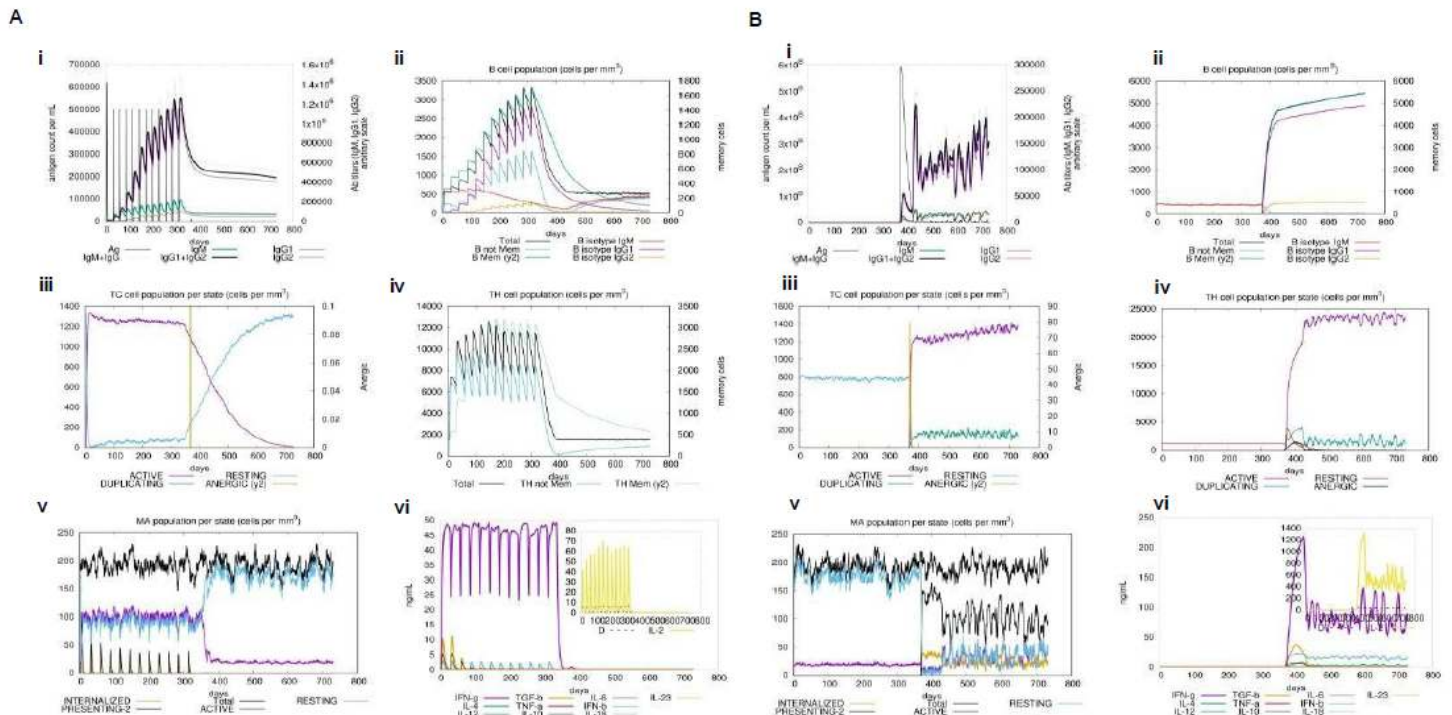


**Figure 11**

In silico immune expression of the vaccine construct. Panel (A) Simulation with vaccine as antigen and later injection of a live-replicating virus. A protective humoral response prevents the later injected virus to growth thus showing the efficacy of the vaccination. (B) Control simulation of the injection with live-replicating virus without prior vaccination. In this case the viral load grows unstopped showing that a naïve host response is not able to eliminate the virus.

## Supplementary Files

This is a list of supplementary files associated with this preprint. Click to download.

- [Supplementaryinformation.pdf](#)